Title
Adaptive Scheduling in Ad Hoc and Cellular Wireless Networks

Author
Tan, Choo Chin

Publication Date
2013

Peer reviewed|Thesis/dissertation

UNIVERSITY OF CALIFORNIA

LOS ANGELES

Adaptive Scheduling in Ad Hoc and Cellular Wireless Networks

A Dissertation Submitted in Partial Satisfaction of the

Requirements for the Degree Doctor of Philosophy

in Electrical Engineering

by

Choo Chin Tan

2013

ABSTRACT OF THE DISSERTATION

Adaptive Scheduling in Ad Hoc and Wireless Cellular Networks

by

Choo Chin Tan

Doctor of Philosophy in Electrical Engineering

University of California, Los Angeles, 2013

Professor Izhak Rubin, Chair

Next generation 4G LTE-Enhanced wireless cellular networks are designed to provide broadband high speed transport services to mobile users. Due to the scarcity of spectral resources that can be employed, it is essential for the networks to engage in multi-dimensional adaptations in the dynamic assignment of wireless access resources. The robustness of wireless cellular networks is also of importance, since failures or degradations of network elements inevitably lead to major network service disruptions. Thus, efficient failover mechanisms are required to handle this scenario.

This dissertation introduces efficient adaptive scheduling algorithms for multicast and unicast downlink transmission operations in cellular wireless networks. Under multicast operations, the newly developed adaptive power scheduling algorithms enable base stations to coordinate, on a spatial-TDMA basis, the transmission of multicast packets to identified mobile users. This joint scheduling and power control problem is shown to be representable as a mixed-integer linear

programming model, which is NP-hard. Consequently, heuristic algorithms of polynomial complexity are developed for solving the problem in a practical manner. These algorithms are shown to yield excellent throughput rate performance behavior, and to lower communications energy consumption levels. Under unicast networking operations, we introduce dynamic scheduling algorithms that allow busy base stations to make use of resources that remain under-utilized by lightly loaded neighboring base stations. Such a dynamically employed resource sharing mechanism is shown to provide significant enhancement to the system throughput capacity. Furthermore, the algorithms exhibit efficient performance behavior under failover scenarios.

We also study multicast networking in wireless ad hoc networks. We consider an energy-aware mobile backbone network architecture under which certain nodes are dynamically elected to act as backbone nodes. Each backbone node manages the wireless access network that it controls, providing for the transport of messages from/to mobile clients and the Bnet. We introduce the concept of performing multicast packet distributions among the mobile ad hoc wireless network nodes using a hybrid multicast protocol. We show that the hierarchical Bnet based hybrid multicast architecture leads to efficient system performance behavior under different operational scenarios examined.

The dissertation of Choo Chin Tan is approved.

Kung Yao

Bruce L Miller

Lieven Vandenberghe

Izhak Rubin, Committee Chair

University of California, Los Angeles

2013

Table of Contents

Biography

Choo Chin Tan received his B.Sc. and M.Sc. degrees in electrical engineering from Purdue University in 1998 and San Jose State University in 2002, respectively. His research interests include adaptive scheduling and routing algorithms, network modeling and analysis, self-organization wireless networks and wireless mobile ad-hoc networks. His is currently working for ViaSat Inc. in Carlsbad.

1 Introduction

Next generation cellular wireless networks, such as those defined by the 4G LTE-Enhanced architecture, are designed to provide broadband high speed transport services (both multicast and unicast) to mobile users. Under multicast operations, we develop adaptive-power and rate scheduling algorithms that enable base stations to coordinate, on a time-division basis, the transmission of multicast packets to identified multicast group clients, for scenarios under which a prescribed code rate is employed. Such mechanisms can be implemented by 4G Long Term Evolution (LTE) systems using Multimedia Broadcast Multicast Services (MBMS), meshed WiFi networks, or mobile backbone based ad hoc wireless networks. We show that the joint scheduling and power control problem can be represented as a mixed-integer linear programming model, which is NP-hard. Consequently, we present three computationally efficient heuristic algorithms of polynomial complexity that jointly determine the multicast schedule, the underlying base station transmit power levels and the set of client nodes that are addressed by each transmitting base station in each time slot. Further enhancement in throughput rate performance is achieved by using an *m-linking* operation under which, when feasible, a client may be directed to receive multicast packets transmitted by a base station which is not the same one that it is associated with. The use of power adaptations in our algorithm leads to lower communications energy consumption levels.

Under unicast operations in wireless cellular networks, we develop dynamic scheduling algorithms derived through coordination among base stations, incorporating into the operation cross-layer code rate adaptations that are achieved by the dynamic selection of the proper modulation/coding schemes (MCS). The algorithms are designed for handling failovers and heterogeneous traffic loading levels in cellular wireless networks. When the system is

symmetrically loaded, or when it is highly loaded such that all base stations are kept fully engaged, a sector oriented time-reuse *static* scheduling protocol is utilized. In turn, when the system is asymmetrically loaded, such that in each neighborhood there may be a cell (or several such base stations) that is heavily loaded while the other neighboring base stations are lightly loaded, the use of the static scheduling algorithm is much improved by the use of our *dynamic* scheduling algorithm. The latter is based on the following concept. A heavily loaded base stations is permitted to execute downlink message transmissions to mobiles that are located in sector i, by not only using its *native* allocated time slot i, but also making use of *non-native* time slot j, where $j \neq i$. The latter transmissions can only be executed when they do not interfere with downlink transmissions of other base stations that would take place during their allocated native time periods. The dynamic mechanisms lead to significant enhancement of the system throughput capacity, and exhibit efficient behavior under the failure of a base station node, whereby neighboring base station nodes adapt their scheduling operations to provide coverage to mobiles that are located in the area of the failed cell.

For mobile wireless ad hoc networks, the synthesis of efficient and scalable multicasting schemes is a challenging task. We develop a multicast protocol that employs a dynamically synthesized energy-aware Mobile Backbone Network (MBN) to achieve efficient message distribution among members of multicast groups. Keeping backbone nodes continuously awake, the synthesized backbone network is used to distribute multicast packets to session receivers. This hierarchical network architecture and multicast protocol is scalable and achieves low control overhead and high throughput and energy-aware throughput-per-unit power performance efficiency. The employed dynamic backbone synthesis mechanism incorporates a power saving mechanism that allows inactive nodes to transition into sleep state to conserve energy. The

hybrid backbone based protocol can be adjusted to operate in a backbone flooding mode or in a backbone extended-tree distribution mode.

The dissertation is organized as follows. Chapter 2 presents adaptive routing protocols for multicasting in energy-aware backbone based wireless ad hoc networks. Chapter 3 presents joint scheduling and power control algorithms for multicasting in cellular wireless networks. Chapter 4 presents the dynamic unicast scheduling algorithms for cellular wireless networks whereby different regional base station nodes carry different levels of traffic loads, for the efficient support of pre-failure and post-failure operations. Conclusions are presented in Chapter 5.

2 Multicasting in Energy Aware Mobile Backbone Based Wireless Ad Hoc Networks

Mobile ad hoc networks (MANETs) are dynamic self-configurable wireless networks, which has no fixed infrastructure or centralized administration. These characteristics make MANETs suitable for mission-critical applications such as disaster recovery and tactical deployment. However, nodes in a MANET can move arbitrarily, resulting in frequent and unpredictable network topology changes, making conventional routing and multicast mechanisms designed for wired networks and fixed-infrastructure mobile networks both ineffective and expensive. Moreover, most wireless ad hoc or sensor networks are bandwidth limited, and many include nodes that are highly energy limited. For these reasons, the development of routing and multicast protocols for MANET is extremely challenging.

Multicasting is an operation that allows the distribution of a message to multiple recipients that are members of a designated multicast group, and has been identified as one of the key application classes for MANETs. As a result, various MANET-specific multicast protocols have been proposed [1], [2], [3], [4]. A survey of these protocols and their performance comparisons are discussed in [5]. These protocols typically construct a tree or mesh structure that is used to distribute messages to multicast group members. Generally, these implementations impose scalability and efficiency limitations for large networks since they employ protocols that are based on a flat-topology networking architecture. When nodal mobility and/or the number of multicast group members increase, traditional tree-based or mesh-based methods become inefficient due to the excessive number of control messages needed for maintaining the multicast forwarding structure. This control overhead will cause an increase in packet contention and collisions, resulting in network performance degradation. In [6], we have introduced mobile

backbone-based multicast protocols to solve this scalability issue. Using a dynamically synthesized backbone network, we have a hierarchical networking architecture that enables a multicast protocol to achieve low overhead and high transmission efficiency.

Due to the diversity of applications of ad hoc networks, it is a challenging task to design a single algorithm that can operate efficiently across a wide range of operational conditions and network configurations. For example, we have shown in [7] under the MBN architecture that flooding of multicast messages across the backbone network as a mean of multicasting (by delivering the packet to all the nodes in the network regardless of who the intended recipients are) does perform better than mesh-based multicasting under high mobility and with large number of multicast receivers/group members that scatters across the network. This is because flooding does not require the creation and maintenance of the multicast structure, and the inherent redundancy in multiple data transmissions provides extra robustness under mobility. However, the properties for flooding render it an unsuitable choice in scenarios with small number of multicast receivers, and a multicast forwarding structure is desirable. Thus, we propose a hybrid multicast protocol with multi-behavioral mode of operations. By combining particular properties of each type of multicast forwarding strategy into a single framework, we are able to capitalize on each algorithm's strengths under different network scenarios.

Many practical applications of MANET include nodes that are highly energy limited. To preserve acceptable operational lifetimes for these nodes, it is essential to employ multicast protocols that minimize nodal energy consumption while providing reliable network transmissions. Existing energy conservation mechanisms for ad hoc networks can be classified into the following two categories: active and passive. Active energy conservation schemes reduce energy consumption of a node based on optimization procedures instead of turning off its

radio module. Various energy-efficient multicasting schemes [11], [12] have been introduced to find a minimum-energy multicast tree such that the total energy cost is minimized by adaptively adjusting the radio transmission power levels, whereas maximum lifetime multicast schemes [13], [14] aim to discover an optimal evenly-distributed transmission load to balance the energy dissipation among nodes to maximize the operational lifetime of the network. However, these optimization-based energy conservation schemes only consider the static ad hoc network scenario. On the other hand, passive energy conservation schemes reduce energy consumption of a node by turning off its radio module when it has no communication activity. The radio module can be modeled to dynamically operate in four key states: sleep, idle, receive, and transmit states. Table 2-1 illustrates the energy consumption rates of the Lucent WaveLAN 802.11b network interface card, as measured by L. Feeney et al. [15]. The energy consumption of a nodal entity when it resides in idle state is only slightly lower than that observed when it resides in receive state. Thus, the energy consumed in idle state constitutes a significant part of the total energy consumption and cannot be ignored. As a result, it is crucial from the energy-saving perspective to switch the radio module to sleep state when a node is not in use, rather than only depending on plain active energy conservation schemes.

Table 2-1:

Energy Consumption Rates of the Lucent WaveLAN 802.11b Network Interface Card

Sleep	Idle	Receive	Transmit
47.4 mW	739 mW	901 mW	1.35 W

The objective of this paper is to present a hybrid multicast protocol that employ a dynamically synthesized Energy-Aware Mobile Backbone Network (MBN) to achieve efficient message distribution among members of the multicast groups. MBN is an extension to the MBN architecture which incorporates a power saving mechanism that allows inactive nodes to

transition into sleep state to conserve energy, and elects nodes with higher energy reserves to act as forwarding nodes to extend the lifetime of the network. The proposed hybrid multicast protocol has multi-behavioral modes of operations and will adapt its behavior under different network conditions to improve performance. Particularly, we look at the following three design dimensions – scalability, adaptability, and power efficiency. We study the throughput efficiency performance of the MBN based multicast protocols through analytical and simulation evaluations. For fair comparison, we have defined and implemented an extended version of ODMRP with power saving mechanism (ODMRP-PS). The specifications and detailed description of ODMRP-PS can be found in the Section 2.6 (b).

The rest of the paper is organized as follows. In Section 2.1, we discuss the related works. In Section 2.2, we provide an overview of the energy-aware mobile backbone network architecture and its topology synthesis algorithm. In Section 2.3, we present the proposed MBN based hybrid multicast protocol. In Section 2.4, we analytically study the performance of the hybrid multicast protocol. In Section 2.5, we present our simulation results and analysis. In Section 2.6, we describe the power savings schemes.

2.1 Related Works

Numerous multicast protocols have been developed for MANETs. Most existing multicast protocols can be classified as either tree-based or mesh-based according to the kind of multicast structure they used to forward multicast packets. Tree-based protocols construct a tree that spans across all members of the same multicast group in which multicast packets are distributed, while mesh-based protocols select a subset of the network nodes to act as a forwarding mesh for the multicast packets to reach the members. In [5], the authors concluded that in general mesh-based protocols, particularly ODMRP, perform better than tree-based approaches. While tree-based

protocols are very efficient, they do not always offer sufficient robustness in the presence of nodal mobility for MANETs. Conversely, mesh-based protocols address robustness and reliability requirements with path redundancy inherent to meshes.

State management of multicast protocols involves timely updating of the multicast routing tables at the selected nodes to maintain the correctness of the multicast routing structure, tree or mesh, according to the current network topology. As nodal mobility and/or multicast group size increase, traditional protocols such as those mentioned above become inefficient since considerable amount of control overhead is needed for state management. In order to address this scalability issue, it is essential to reduce the rate of the control messages. A number of research attempting to reach such a reduction have been conducted, and two of the more effective approaches proposed are the overlay multicast schemes and hierarchical-based multicast protocols.

Overlay multicast schemes [4], [16] build a virtual infrastructure to form an overlay network spanning all multicast member on top of the physical network. Each link in the virtual infrastructure is a unicast tunnel in the physical network. To achieve low control overhead, these schemes restrain all multicast functionality and protocol states within the group member nodes, i.e. they do not require any support from the non-member nodes. In addition to that, these schemes do not need to track nodal mobility since this is totally handled by the underlying unicast protocol. However, efficiency is an issue since it is very hard to prevent different unicast tunnels from sharing the same physical links due to the mismatch of the virtual infrastructure and the physical topology under mobility. This results in physical links forwarding the same packet multiple times. Moreover, overlay multicast schemes suffer from inefficient transmissions among densely located multicast members since multiple unicast transmissions are required

instead of just using a single broadcast, incurring high bandwidth waste. These disadvantages were overcome through the creation of single-hop clusters to manage dense multicast members to reduce overhead by broadcasting in these clusters, and placing restriction on multicast sources to deliver multicast data only to the cluster leaders through an overlay multicast tree.

Hierarchical-based algorithms [19], [20] use a distributed election process to select a subset of nodes to form the virtual backbone of the network. The maintenance of state information and multicast data forwarding are kept only in the backbone nodes. Our MBN based multicast protocol falls in this category as well, and the detailed description of the protocol can be found in Section 2.4.

Most of the energy-efficient protocols proposed in the literature [11], [12] were focused on controlling the construction of the forwarding path so that it includes nodes that have the highest residual battery power among different possible paths or to consume the least energy along the selected path. In many of these papers, the min-max algorithm was used as a mean to find the best path with maximum residual energy. However, as observed from previous discussion, it is crucial from the energy-saving perspective to switch the radio module to sleep state when a node is not in use, rather than only trying to minimize the total transmission power consumption of nodes. Thus, the MBN architecture provides a structure to manage node sleeping/suspending schedule effectively to further extend the lifetime of nodes.

To the best of our knowledge, only a limited number of works look at adaptive, multi-behavioral multicast protocols. In [22], the authors proposed an adaptive, multi-behavioral multicast protocol which uses different modes of operations that are either proactive or reactive to improve network performance. The algorithm dictates that a node chooses a mode of operation depending on different considerations such as residual energy, mobility level and/or

vicinity density level. Our MBN based hybrid multicast protocol differs from the above work in several aspects. Firstly, our MBN architecture provides a hierarchical network structure to solve the scalability issue. Secondly, the different mode of operations in our algorithm focuses on achieving good data forwarding efficiency by changing its behavior to adapt to the different underlying network scenarios. Thirdly, our algorithm contains a power savings mechanism to achieve energy conservation.

2.2 Energy-Aware Mobile Backbone Network

Under our Energy-Aware Mobile Backbone Network (MBN) architecture, which was first introduced in [9], nodes belong to one of these two classes: regular nodes (RNs) and backbone capable nodes (BCNs). The backbone network is constructed by dynamically electing BCNs to act as backbone nodes (BNs) and forming backbone links to interconnect neighboring BNs. Such a structure is illustrated in Fig. 2-1. Under the MBN concept studied in this paper, nodes that currently do not serve as BNs, and also do not serve as relays for traffic flows are switched into sleep mode. In turn, we assume here that nodes that serve as BNs are kept continuously awake for as long as they are elected to act as backbone nodes. The subnetwork that consists of large solid circles interconnected by thick solid lines represents the backbone network. In general, the backbone network is designed so that it involves a sufficient but not excessive number of BNs while providing wide topological coverage. This ensures a level of backbone connectivity in response to communications link failures, nodal failures and mobility. Assuming a connected network layout, each BCN is a single hop away from at least one BN, and each RN can reach at least a single BN by traversing a path that consists solely of RNs. We note that for the special case under which all nodes are BCNs, with the assumption that a connected covering exists, the backbone network will serve as a Connected Dominating Set of the network graph. Each BCN or

RN is required to associate with a single BN. A BN and its associated BCNs and RNs will form an access network (Anet). The Anets are represented by the dotted circles in the figure.

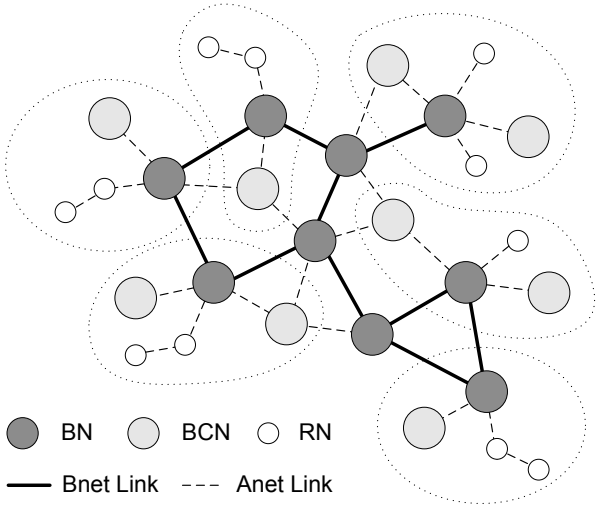

Fig. 2-1. The Mobile Backbone Network Architecture

The fully-distributed topology synthesis algorithm employed herein is a modified version of the one presented in [6]. Every node periodically sends *hello* messages to its direct neighbors. A backbone network is formed by dynamically electing BCNs to act as BNs. Every BCN associates with one BN that is its direct neighbor. A BCN will convert to BN state if it needs to provide client coverage for its BCN or RN neighbors or to enhance the local connectivity for its BN neighbors. A BN will convert back to BCN state if it finds that it is not needed for both client coverage and local backbone connectivity purposes. These conversion decisions are based on the weight of the nodes, which could be calculated based on nodal ID, or nodal degree, nodal energy levels, and/or stability metrics such as nodal speed. Please refer to [10] for a detailed description of the conversion algorithm. A regular node (RN) that does not have a BCN neighbor, will reach its associated BN through a multi-hop path that traverses intermediate RNs. We further note that the speed of a node, as well as its available energy level is included when calculating the nodes' weight vector. In this manner, we aim to elect BNs that tend to move at slower pace to avoid

frequent connectivity breakups and to also reduce energy dissipation involved with re-elections (and possibly induced retransmissions) that are caused by such breakups.

Consider a multicast session operation under our MBN based multicast scheme. A BN is regarded as a source BN if it is the source node for a multicast group, or if there exists at least one source node in its associated Anet. For a non-BN source node (that is, a node that is residing in the Anet), a protocol similar to IGMP can be utilized to handle the communication between the source node and the associated source BN. For most of the flat-topology based proactive multicasting algorithms, a multicast source node is responsible for constructing and maintaining the multicast forwarding structure. Our hierarchical-based multicast protocol reduces the control overhead incurred in this manner since multiple source nodes from the same multicast group may associate to the same source BN, in which the latter acts as a "router" for these source nodes; i.e., different source nodes that associate with the same source BN can utilize the same multicast forwarding structure. On the other hand, a BN is regarded as a destination BN if it is the intended recipient for a particular multicast group. This is the case if there exists at least one multicast group recipient in the Anet managed by this BN (including a recipient that is direct attached to the BN). The non-BN multicast receivers can communicate with their corresponding destination BN using a protocol similar to IGMP. A multicast packet for a particular multicast group is distributed through the multicast forwarding structure from the source BN to the corresponding destination BNs, and the destination BNs are responsible to distribute the multicast packets in their own Anets.

We incorporate a power saving mechanism into the MBN architecture to conserve energy by allowing inactive nodes that are not involved in multicasting operation to transition into sleep state. Under this MBN power saving scheme, each BN is kept continuously awake to coordinate

the sleeping/suspending schedules among its Anet clients, i.e. the local non-elected BCNs and RNs, if any, that have associated with it. As implemented by IEEE 802.11 (when operating in a power saving mode), each BN transmits a beacon message at the start of each super frame period targeted to its Anet clients. Since the beacon message is used to pass control and management information, the beacon period is thus identified as the control and management (C&M) period. All nodes wake up periodically at the beginning of each super frame and stay awake during the C&M period. Non-backbone nodes that are not involved in packet transmission enter the sleep state after the common C&M period. The specification and detailed description of the MBN with power saving mechanism is given in Section 2.6 (a).

2.3 MBN Based Hybrid Multicast Protocol

Under our proposed MBN based hybrid multicast protocol, the source BN is responsible for initiating (and updating) the selection of the multicast forwarding structure to utilize for distributing its multicast packets to the respective receivers. The source BN will periodically initiate a query action to determine which operational mode to employ, based on existing multicast group membership information and underlying network conditions. The two possible multicasting operational modes that our hybrid multicast protocol can operate in are the Backbone Network Flooding Multicast operation, and the Extended Shortest Path Multicast Tree operation. In each mode, a distinct multicast forwarding structure is employed for the distribution of multicast group messages.

The determination of which operational mode to activate at a given time instant for the hybrid multicast protocol is based on using mobility level, traffic load level and distribution scope level thresholds. Each node is assumed to be able to monitor its mobility speed level by employing a suitable mechanism [17], and to measure the average mobility speed level in its

vicinity. This can be done, for example, by extracting the nodal speed information contained in the *hello* messages received from its 1-hop neighbors. Each source BN in a multicast session can determine its distribution scope during the conduct of its periodic query actions. At such a time, the source BN floods a *QUERY* message within the backbone network. When a destination BN receives the *QUERY* message, it responds with a *REPLY* message to indicate that it has multicast recipients in its Anet. Based on the number of *REPLY* messages received, the source BN will be able to determine the fraction of BNs within the backbone network that have multicast clients for the underlying multicast group. We denote the mobility speed threshold as *M_TH*, the traffic load level threshold as *TL_TH*, and the distribution scope threshold as *DS_TH*. These thresholds dictate the choice of the operational mode that a source BN selects and deploys (for the underlying multicast session), using the selection criteria employed by our hybrid multicast protocol. In the following, we first describe the characteristics of the two modes of operation, and then provide a detailed description of the selection criterion.

2.3.1 Mode 1: Backbone Network Flooding Multicast Operation

Consider a time frame period and a multicast group for which such an operation is performed. Multicast messages belonging to this multicast group are flooded across the backbone network. Thus, each BN that receives a multicast message that it has not yet forwarded will proceed to forward it to its neighbors. Furthermore, each BN that has clients that are current members of the underlying multicast group is responsible for copying the multicast packets of interest and distributing them to these clients across its access net. Flooding provides several intrinsic advantages. Firstly, it is easy to implement since it does not require the creation and maintenance of any multicast structure in the backbone network. Secondly, the inherent property of flooding leads to many redundant data transmissions, providing extra robustness under nodal

mobility. Thirdly, since multicast messages are relayed only by BNs in the backbone network, the rate of redundant packet transmissions in the network is reduced and the broadcast storm problem [8] is alleviated. We note however that multicast messages are delivered to all BNs in the network regardless of which BNs are associated with clients that belong to the underlying multicast group. Such a wide distribution process can lead to higher channel utilization rates. In particular, this operation induces lower bandwidth efficiency for scenarios under which group members are not widely distributed over the network. In turn, one expects this operation to yield higher performance behavior when group members are widely distributed and when higher mobility rates induce frequent changing and spatially widely distributed associations of mobile nodes with the BNs.

2.3.2 Mode 2: Extended Shortest Path Multicast Tree Operation

For scenarios when the distribution scope for the underlying multicast group is small or limited, it is desirable to utilize a more bandwidth-efficient multicast forwarding structure than that employed by the flooding mechanism. A multicast tree is an effective distribution structure in this case. However, a tree is easily broken under nodal mobility. To offer more robustness to the tree structure, we hereby introduce the following scheme, identified as the Extended Shortest Path Multicast Tree operation. Under this scheme, additional forwarding nodes are selected and grafted into the original multicast tree. These nodes are referred to as the Extended Tree Nodes (ETN), and when combined with the original Tree Nodes (TN) will create an extended multicast tree rooted at the source BN. Under the protocol presented here, the ETNs are selected based on the examination of a number of specified redundancy rules, used to avoid having too many ETNs. The extended multicast tree is then used for the distribution of messages across the backbone network from the source BN to the destination BNs that are members of the underlying

multicast group. A detailed description of the extended multicast tree construction algorithm is listed below.

Step 1: Construction of a source-based shortest path multicast tree

An active multicast source BN floods a *QUERY* message within the backbone network. When a destination BN receives the *QUERY* message, it responds with a *REPLY* message to indicate that it is a member of this multicast group (i.e., it has, within its Anet, receivers that have joined the group). The *REPLY* message is forwarded back to the corresponding source BN using the reverse path forwarding mechanism, thus creating a source-based shortest path multicast tree that connects the source BN to the multicast session members' destination BNs.

Step 2: Grafting of extended tree nodes

Each backbone node is assigned a weight that is equal to the number of its 1-hop tree backbone-node neighbors.

(i) If a node has at least two 1-hop TN neighbors, it is defined as an ETN candidate.

(ii) When an ETN candidate has any two TN neighbors that are not commonly shared with any other ETN, then it is selected as an ETN.

(iii) When an ETN candidate has any two TN neighbors that are commonly shared with at least one other ETN candidate, the respective candidates compare their weights and the node with the highest weight elects itself to be an extended tree node. If several candidates assume the same highest weight level, the nodal ID is used to resolve the tie, e.g. the candidate node with the highest nodal ID is selected as the ETN.

We note that when a source-based shortest path multicast tree scheme is applied to a flat topology network, high control overhead and algorithmic complexity levels are observed as the

number of multicast source nodes increases. Conversely, our MBN base multicast protocol uses a backbone network to overcome these disadvantages: (i) only BNs are capable of becoming forwarding nodes in the multicast tree, reducing the number of nodes that participate in the formation and maintenance of the multicast forwarding structure, which leads to substantial control overhead reduction; (ii) flooding of *Query* messages during the multicast tree construction phase is confined only to the backbone nodes, resulting in greatly reduced respective control overhead; (iii) multiple multicast sources attached to the same source BN construct/share a single multicast tree; (iv) when a destination BN discovers that there is a new multicast recipient association in its Anet, it will construct a link/branch to the closest forwarding node that is a member of the same multicast group through the reverse path forwarding mechanism. Thus, unlike ODMRP, newly acquired multicast members do not need to wait for the periodic refresh/update to start their multicast sessions.

Although this mode of operation is more complicated than flooding, in that it requires maintenance of the extended tree structure, it leads to a more bandwidth efficient operation when multicast group members are not widely distributed. In Fig. 2-2, we provide illustrations of tree and extended tree layouts.

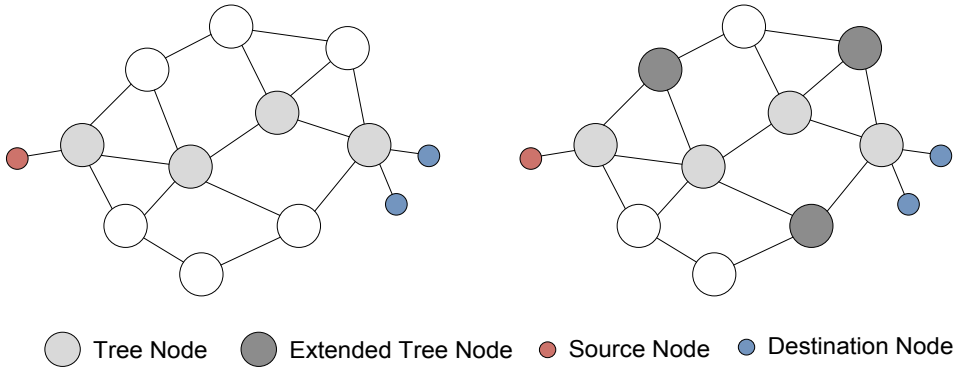

(a) Original Multicast Tree (b) Grafting of Extended Tree Nodes

Fig. 2-2: The Overall Operation of Creating the Extended Multicast Tree

We employ both modes of operation in our proposed hybrid multicast protocol. When a source BN acts to construct a new multicast forwarding structure, a selection of the operational mode (either BFMA or E-SPMT mode) for this structure is made. The selection criteria are based on the values of the three threshold levels, as described in the following algorithm.

Algorithm 3-1: Hybrid Multicast Protocol Selection Criteria

```
if Mobility < M_TH then
    if Distribution Scope < DS_TH then
        Mode selection: E-SPMT
    else
        if Traffic Load < TL_TH then
            Mode selection: BFMA
        else
            Mode selection: E-SPMT
        end if
    end if
else
    if Distribution Scope < DS_TH then
        if Traffic Load < TL_TH then
            Mode selection: BFMA
        else
            Mode selection: E-SPMT
        end if
    else
        Mode selection: BFMA
    end if
end if
```

When the average nodal mobility is high, it is preferable for a multicast session to operate in the BFMA mode, regardless of the distribution scope, since it is hard to maintain a multicast forwarding structure when the underlying network topology changes frequently. However, an exception case would be when a multicast session has limited distribution scope with high traffic

load. The hybrid multicast protocol is then set to operate in the E-SPMT mode even though the extended multicast tree is not robust (especially for the scenario under which the rate of network topological changes exceeds the rate of periodic update of the E-SPMT protocol) since flooding in the BFMA mode under high traffic load consumes high bandwidth and will lead to saturation (or close to saturation conditions) of the network communications capacity resources. In this case, we illustrate in Section 2.5 that operating in the E-SPMT mode improves the overall attained network throughput rate.

When the distribution scope of a multicast session is limited and the average nodal mobility is low, the multicast session is set to operate in the E-SPMT mode. This is especially true when the traffic load of the multicast session is high since utilizing an efficient multicast forwarding structure to distribute multicast messages is expected, under current conditions, to improve the realized network throughput rate. In turn, when the distribution scope is high, the hybrid multicast protocol chooses to operate in the E-SPMT mode when the traffic load is high (to increase the bandwidth utilization efficiency of the operation), and to operate in the BFMA mode when the traffic load is low. In Section 2.5, we observe, for the illustrative networking scenarios when operating under lower traffic loading rates, that constructing and maintaining an extended multicast tree is less efficient (in terms of throughput) than using a backbone flooding scheme, when the distribution scope is sufficiently high.

2.4 Performance Analysis

The objective of this section is to present key performance measures for our proposed multicast protocols. We are able to mathematically characterize the bit-per-joule performance for the algorithms under evaluation. Our analysis proceeds as follows: we first examine the backbone network size and multicast forwarding structure to obtain an expression for multicast

efficiency. Then, we evaluate the number of active nodes and energy consumption level for different multicast protocols to obtain an expression for bit-per-joule throughput efficiency.

2.4.1 Backbone Network Size

For analytical and simulation evaluations, we use a disk covering approach to approximate the minimum size of the Bnet. Such a lower bound estimate is obtained under the assumption that we could choose the optimum locations of the BNs to cover the entire area. Kershner [21] showed that no arrangement of circles could cover an area ore efficiently than the hexagonal lattice arrangement, with the nominal data link communications range of a node, r_c determines the length of a hexagon's side. For example, the Bnet for a 1500m × 1500m operational region with an effective radio transmission range of 300m is illustrated in Fig. 2-3. The Bnet then forms a Connected Dominating Set (CDS) since any node located inside a hexagon is reachable from at least one of the vertex nodes of the hexagon. Using this arrangement, the minimum number of BNs required to form a Bnet to cover the entire $D \times D$ square region ($D > r_c$) has been shown to be approximated as $0.769 D^2 / r_c^2$. Thus, the minimum Bnet size for the illustrative example is approximated to be 19 BNs. This lower bound is normally not achievable in a real scenario since BNs are selected from BCNs that randomly roam over the area of operation.

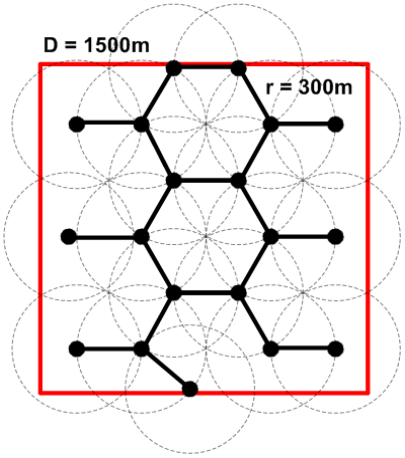

Fig. 2-3. The Minimum-Size Backbone Network for a 1500m × 1500m Region

2.4.2 Network Model

Topological and Physical Layer Parameters: Consider an ad hoc network that consists of N nodes, each of which is capable of transmitting packets across its wireless channel at a data rate of R bits per second [bps]. To simplify our approximate computation of the spatial reuse factor attainable in a wireless network, we assume the nominal data link communications range to be equal to r_c. [meters]. The latter can be calculated under the given physical layer data (modulation/coding scheme, average SINR at the receivers, targeted bit error rate and transmit power levels), or obtained through simulation measurements. For a given ad hoc network that occupies a geographic area A, we assume that the number and/or distribution of BCNs are sufficient to provide global coverage for this region of operation. Under a prescribed loading and mobility scenario, and for a given backbone topology synthesis algorithm, let N_B denote the average number of backbone nodes that are needed to provide complete one-hop coverage.

Traffic Parameters: We consider a network that includes multiple active multicast sessions. Each such session, when active, involves a single source node that stochastically generates a flow of messages that are destined to all members of the underlying multicast session. For simplicity of presentation, we assume each multicast session to last for a random duration that is exponentially distributed with mean duration equal to T sec. Once a flow is admitted into the network, its packet generation activity is characterized as a Poisson process. The packet arrival rate of an active multicast session is set to be equal to λ [packets/sec], and the average packet size is L_{data} bits.

MBN Power Savings Parameters: Under the MBN power savings scheme, each node wakes up every T_{frame} seconds and remains awake during a corresponding control period. The duration of the control period is set equal to T_{hello} seconds. The length of a *hello* message for the

ODMRP-PS scheme is set to be equal to L_{hello} = 40 bytes. Under our MBN scheme, since a *hello* message contains additional topological synthesis and power saving information, the length is set to be 110 bytes.

2.4.3 Multicast Forwarding Structure

An ad hoc network can be represented as an undirected graph $G = (V_G, E_G)$, where V_G is the node set and E_G is the set of links between nodes. We assume nodes to employ omni-directional antennas. Using the wireless multicast advantage concept, the transmission of a multicast packet by a node is received by all of its direct neighbors, though some receptions may be successful while others may not. Let $G_M = (V_M, E_M) \subset G$ be the multicast subnetwork that is constructed by the underlying multicast scheme. When a multicast packet is transmitted across a designated G_M, only nodes consist in V_M will retain and forward the packet. The number of forwarding nodes in a multicast subnetwork is $|V_M|$. For our MBN based multicast scheme, a multicast packet that is intended for k_1 multicast group members will be distributed through the subnetwork from the source BN to its k_2 destination BNs (whereby each of the latter manages an Anet that contains at least one single group receiver, such that $k_2 \leq k_1$). Note that destination BNs will distribute the packet to their own Anets. Let $G_{Bnet} = (V_{Bnet}, E_{Bnet})$ be the backbone network graph, where V_{Bnet} consists of all BNs and $|V_{Bnet}|$ be the number of BNs in the Bnet. Since $G_M \subset G_{Bnet}$, the upper bound for the number of BNs that can be selected to form the multicast subnetwork is $|V_M| \leq |V_{Bnet}|$.

2.4.4 Average Number of Awake Nodes

For MBN base multicasting, all BNs must be awake all the time. The rest of the nodes (BCNs and RNs) will be in sleep state unless they are the multicast source or receiver nodes. Thus, the average number of active nodes for MBN base multicasting, N_a is:

$$N_B \le N_a \le \min\left(N_B + \gamma\left(N_R + N_S\right), N\right), \tag{2-1}$$

where γ represents the probability that a sender or a receiver is not a BN, N_S denotes the number of multicast source nodes and N_R is the number of multicast receivers. Conversely, for ODMRP-PS, we derive the average number of awake nodes through simulation.

2.4.5 Energy Consumption Rate

A node is said to be awake when it is not in a sleep state. The energy consumption rate contributed by data flows consists of two key components. The first component is contributed by nodes during periods that are transmitting packets, whereas the other component is contributed by nodes that are awake (either in idle or receive state) but are not in the transmission mode. For our approximate analysis, we assume the energy consumption rates for a node that is in the receive state is the same as that incurred when it is in the active idle state. Also, we neglect the energy consumption rate when a node is in sleep state, since it is significantly smaller than the energy consumption rates incurred when a node is in other states.

Denote the energy consumption rate at a node that is in awake non-transmission state by W_r watts. Denote the fraction of time that an awake node stays in transmission state by ρ. Let N_a represent the average number of awake nodes in the network at any time during steady state. The energy consumption rate contributed by nodes that are in awake non-transmission state is equal to $N_a W_r(1-\rho)$. Denote the energy consumption rate at a node when it resides in transmission state by W_t watts. Since the average number of admitted forwarding-broadcast is equal to N_f, the energy consumption rate contributed by nodes that are in transmission state is given by $N_f W_t\left(\lambda L_{data}/R\right)$. The average energy consumption rate contributed by data flows, W_f is thus given by the following expression:

$$W_f = N_f W_t \lambda L_{data}/R + N_a W_r(1-\rho). \tag{2-2}$$

We note that at steady state the overall transmitted message bit rate is equal $N_f \lambda L_{data}$ bps. Hence, the average fraction of time that an awake node stays in transmit state is given by $\rho = N_f \lambda L_{data} / N_a R$. Consequently, we obtain the following equation:

$$W_f = N_a W_r + N_f \lambda L_{data} \left(W_t - W_r \right) / R . \tag{2-3}$$

We proceed to estimate the energy contributed by nodes during the control and management (*C&M*) period. Let ε represents the fraction of time a node stays in the *C&M* state, and ζ denotes the fraction of time a node is transmitting control messages during the *C&M* period. In our simulation, when a node has 20 neighbors, the size of its *hello* message is determined to be 110 bytes. Thus, the transmission time of a *hello* message is equal to 0.44 ms, under a prescribed data rate of 2 Mbps. We have adopted in our simulation a *hello* period duration of 50 ms and this has proven to be sufficiently long for accommodating the *hello* message traffic load generated in our simulations under a prescribed nodal density. The average energy consumption rate contributed by control overhead, $W_{control}$ is expressed by:

$$W_{control} = \varepsilon \left[\zeta W_t + (1 - \zeta) N W_r \right]. \tag{2-4}$$

2.4.6 Bits-Per-Joule Performance

The bit-per-joule throughput efficiency performance for ODMRP-PS and MBN based multicast protocols is concluded as the ratio between the total network throughputs (*TH*) received by the receivers and the total average energy consumption rate. Since ζ from (4) is a very small number, the expression can be simplified to be:

$$\chi = \frac{TH}{W_f + W_{control}} = \frac{TH}{(1-\varepsilon)\left[N_a W_r + \rho (W_t - W_r) \right] + \varepsilon \left[N W_r \right]} . \tag{2-5}$$

This analytical expression is used to compare with the bit-per-joule simulation results presented in Section 2.5.

2.5 Simulation Results and Analysis

The simulation models of the proposed multicasting schemes were implemented in QualNet. The Distributed Coordination Function (DCF) of IEEE 802.11b is used as the MAC layer protocol. The channel capacity is 2 Mbps and the effective radio transmission range is 300m. The multicast protocol parameter values are shown in Table 2-2. Several refresh intervals were examined for ODMRP and the optimum value was selected to be 3s to achieve low overhead while maintaining a good packet delivery ratio. The general settings for the simulation scenarios are listed in Table 2-3. All nodes were placed randomly within the area of operation. The inter-arrival time of data packets for each sender is exponentially distributed, with an average of 0.5s. The radio power levels are selected to be W_r = 900mW and W_t = 1300mW. A single multicast group activity is simulated. The group is modeled by specifying the number of sending and receiving participants and then selecting group members at random. Member nodes join the multicast session at the beginning of the simulation and remain as members throughout the simulation.

Table 2-2: Major Protocol Parameter Values

ODMRP	Join-Query Refresh Interval	3 seconds
MBN-TSA	*Hello* Message Interval	1 seconds
E-SPMT	Extended Tree Refresh Interval	10 seconds

Table 2-3: Simulation Environment

Simulation Duration	300 seconds
Network Dimension	1500m × 1500m
Number of Nodes	100
Average Data Packet Size	512 bytes

The simulation metrics that we have used are listed below. They all represent the sample mean estimates of the corresponding average values of the performance metrics noted below.

- Packet Delivery Ratio (PDR): The ratio of the number of data packets *actually* received by the receivers versus the *expected* number to be received.
- Data Forwarding Efficiency: The ratio of the number of data packet successfully delivered to the receivers versus the total number of data packets transmitted (including packet retransmissions) across the network.
- Control Overhead: Represents the number of control packets transmitted for each data packet that is successfully delivered to the receivers.
- Bit-Per-Joule Performance: Represents the throughput per unit energy efficiency performance of a multicast protocol.

2.5.1 Multicast Protocol Performance Comparisons

The simulation scenario parameters are given by Tables 3-2 and 3-3. The multicast group is constructed to include 10 receiving nodes and a variable number of sending nodes. A nodal mobility speed of 10 m/s is set. Nodes move according to the *random waypoint* mobility model. The multicast senders produce incoming network flows, each with an average flow rate of 8.2 kbps. Fig. 2-4(a) shows the packet delivery ratio (PDR) obtained by using the multicast protocols under different number of senders. The MBN based multicast protocols introduced in this paper are shown to achieve excellent PDR performance under the prescribed network scenario. In turn, the ODMRP-PS multicast scheme results in rapid performance degradation as the network traffic load increases over a certain threshold. Fig. 2-4(b) shows the data forwarding efficiency. We observe that our MBN based multicast protocols exhibit much better efficiency performance than that displayed by the ODMRP-PS scheme due to the effective use that they make of the

backbone network in limiting the number of forwarding nodes. We also note that in comparing the two MBN based protocols, the extended tree mechanism yields better bandwidth efficiency while achieving somewhat lower delivery ratio. This is explained by noting that while the tree based scheme is more capacity use efficient, the backbone flooding scheme entails an operation that is more robust to nodal mobility.

Generally, the use of a simple flooding scheme would induce the highest level of forwarding overhead. However, hierarchical multicasting schemes such as BFMA restrict the flooding of messages to the backbone network and therefore it leads to a more scalable (and thus bandwidth efficient) operation. The E-SPMT scheme commands the best data forwarding overhead since the algorithm constructs a multicast subnetwork in the Bnet that nominates only a select group of nodes to forward the multicast messages. Comparison of control overhead for the underlying protocols is shown in Fig. 2-4(c), and the results are explained as follows. For the MBN based multicast protocols, the key control overhead component involve the employment of *hello* messages, which are used to maintain the synthesis of the Bnet. The E-SPMT algorithm, in addition to producing the hello messages, also involves the periodic generation of control messages that are used to maintain the integrity of the extended tree structure. Under the ODMRP-PS scheme, a significantly higher rate of control messages is observed, since it involves the use of control messages that are periodically generated and are widely flooded across the network (rather than just across a backbone structure). Also recall that the hello messages generated by a node are broadcasted only once, unlike the wider scope used in distributing multicast structure maintenance messages.

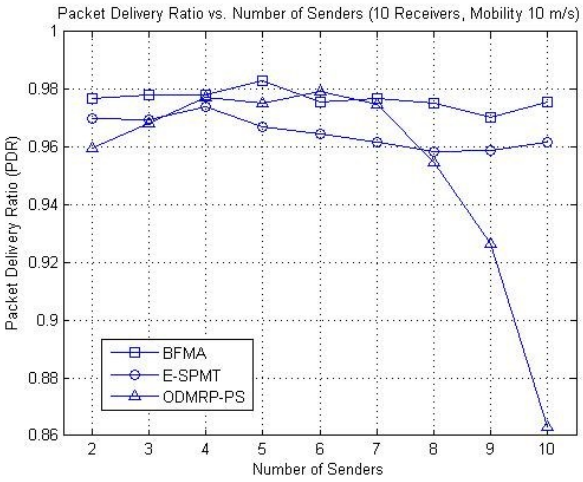

Fig. 2-4(a): Packet Delivery Ratio

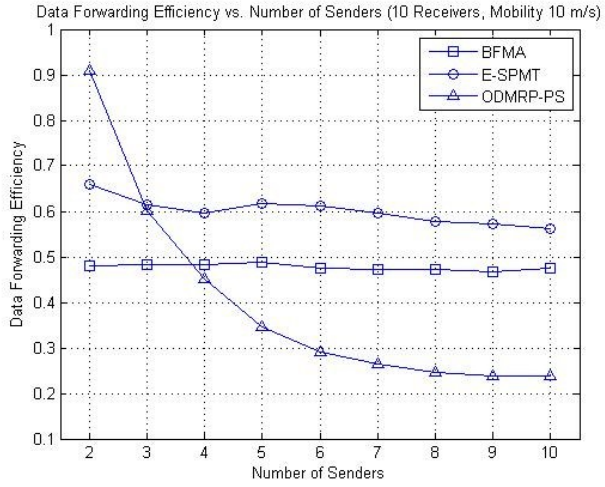

Fig. 2-4(b): Data Forwarding Efficiency

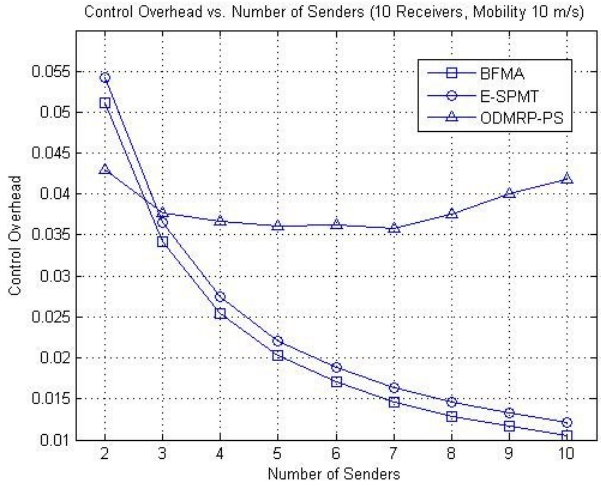

Fig. 2-4(c): Control Overhead

2.5.2 Bits-Per-Joule Performance

The bit-per-joule performance efficiency achieved under the executed simulations, as a function of the number of sending nodes selected for the multicasting group, is plotted in Fig. 2-5. We show the results obtained by the simulation as well as display the performance results obtained by using mathematical expression (2-5). The MBN based multicast protocols are shown to exhibit better performance than that obtained under the ODMRP-PS scheme. This is explained by noting that the MBN based mechanisms use the synthesized backbone structure, which contains a much smaller number of nodes that are kept continuously awake, and therefore consume lower energy resources. When the system offered load is not excessive, both MBN based algorithm yield about the same throughput rate, while inducing about the same energy consumption since in both cases all backbone nodes are kept continuously in the awake state. Therefore, they yield about the same bits per joule performance behavior. As the loading rate of the network becomes sufficiently high such that the throughput capacity attained under the BFMA scheme is reached (observed from the BPJ results obtained by the simulation in Fig. 2-4), the higher throughput capacity rate offered by the E-SPMT scheme leads to higher bits per joule performance when compared with the BFMA scheme. Note that for fair comparison purposes, we have set all examined multicast protocols to use the same control and management (*C&M*) period (during which every node wakes up to exchange *hello* messages); setting it to last for a period of time that is equal to 10% of each super frame duration.

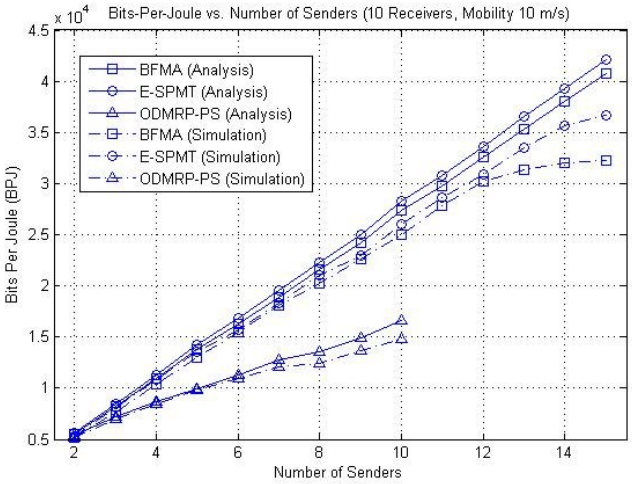

Fig. 2-5: Bits-Per-Joule Performance

2.5.3 Hybrid Multicast Protocol Threshold Values

A simulation approach is used to illustrate the determination of the appropriate threshold values for the hybrid multicast protocol's selection criteria to be utilized for the underlying chosen network. To determine the distribution scope threshold (*DS_TH*), a nodal mobility speed of 20 m/s is set, with a multicast group that consists of 5 sending and 10 receiving nodes. The distribution scope is defined here as the percentage of the estimated total number backbone nodes (identified as destination BNs) that serve multicast session receiver(s) in their access networks. Under the hybrid multicast protocol, a source BN counts the number of *REPLY* messages that it receives from the destination BNs (in response to the source BN's *QUERY* message). The reception of a large number of *REPLY* messages (when referenced to the number of backbone nodes) implies a wide distribution scope, whereby receivers tend then to be sparsely located around the network. Fig. 2-6(a) shows the packet delivery ratio of the multicast protocols under different distribution scopes. For low traffic loads, the BFMA scheme always performs the best regardless of the distribution scope as it provides sufficient robustness to overcome link breakages caused by nodal mobility. Note that in this loading range, the

throughput efficiency attained under the E-SPMT decreases as the scope ratio level increases. This is explained by noting that for higher scope levels, higher fraction of the backbone nodes that are associated with session receivers. Hence, a conversion (due to mobility event) of a BN to non-BN status will more often lead to non-delivery of packets to their destination receivers. For high traffic loads, we observe that the throughput efficiency under the BFMA scheme stays constant with the scope level, although the value achieved is lower under the low traffic load scenario due to increased packet collisions. In contrast, under the E-SPMT protocol, throughput efficiency attained under the E-SPMT decreases as the scope ratio level increases, as higher scope level requires distribution of flows over wider area (and routes) leading to a higher degree of route breakups due to the limited robustness of the extended tree topology. We observe in Fig. 2-6(a) that there is a cross-over point between the corresponding performance vs. scope curves exhibited under the BFMA and E-SPMT schemes. We select the value of the distribution scope at the cross-over point as the distribution scope threshold. For the illustrative scenario, this scope threshold level was measured to be equal to about 30% of the estimated total number backbone nodes.

Next, to determine the nodal mobility threshold (*M_TH*) for the underlying scenario, the maximum throughput rates achievable by the various multicast protocols are measured under different nodal mobility values. A wide distribution scope scenario is selected, with a multicast group that consists of 5 sending and 10 receiving nodes. From Fig. 2-6(b), we observe that for such a static network, the basic SPMT scheme (with a 5 sec. update interval) produces the best BPJ performance result since it offer the highest bandwidth efficiency level. However, as nodal mobility increases, E-SPMT (with a 5 sec. update interval) achieves better BPJ performance than the basic SPMT scheme as the extra nodes are used to construct a more robust extended tree-

based multicast forwarding structure. As the nodal mobility becomes even higher, the BFMA scheme exhibits throughput efficiency that is higher than that obtained under the tree-based multicast algorithms. The value of nodal mobility at the cross-over point between the BFMA vs. mobility performance curve and the E-SPMT vs. mobility performance curve that is obtained when the E-SPMT scheme uses an advantageous update interval level (which is equal to 10 sec in the illustrative scenario) is selected as the mobility threshold. For the underlying scenario, this mobility threshold level has been measured to be 10 m/s. As observed from the same figure, the update interval for the E-SPMT scheme can be optimized by dynamically decreasing it to match a corresponding increase in the nodal mobility level. Under each nodal mobility level, it is desirable to adjust the update interval level of the E-SPMT scheme to reduce the control overhead of the algorithm, and consequently achieve better performance behavior. We observe from the figure that the reduction of the update interval from 10 sec to 5 sec will enhance the performance of the E-SPMT scheme as the mobility speed increases. For the underlying scenario, we note the E-SPMT scheme to yield similar performance around the 10 m/s mobility threshold level under the two update interval levels. Clearly, when managing system parameters under other scenarios and the use of a larger number of candidate update interval parameter levels, similar evaluations may lead to several mobility based intersection points of the BFMA curve with several different E-SPMT curves, each of which corresponds to different values of the update interval that is set to yield enhanced performance at the corresponding range of nodal speed levels.

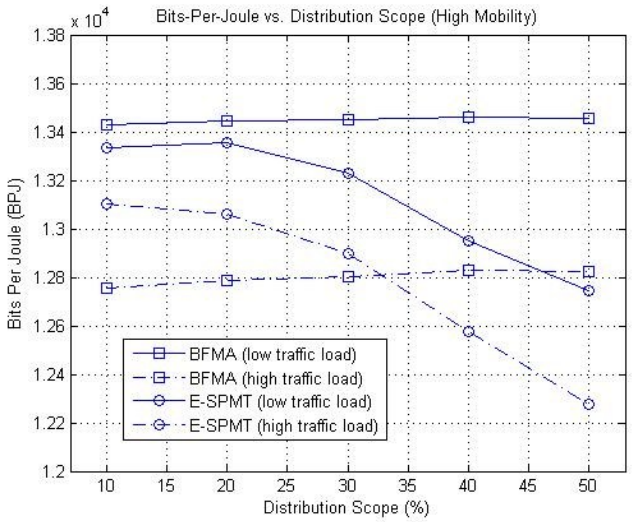

Fig. 2-6(a): Finding distribution scope threshold (*DS_TH*)

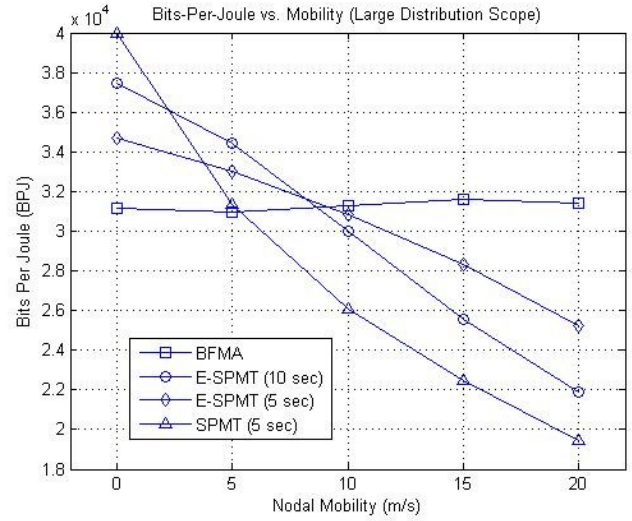

Fig. 2-6(b): Finding mobility threshold (*M_TH*)

2.6 Power Savings Schemes

A. MBN Power Saving Scheme

In this section we provide a detailed description of the MBN power saving scheme. The specifications for this scheme build on top of the operation of the IEEE 802.11 power saving mode and the *hello* message exchange process used by our topology synthesis algorithm (TSA), which the detailed description of the algorithm can be found in [10]. Under TSA, each node

periodically issues *hello* messages to learn its link-layer neighbors. In our scheme, a node includes wake up notification (corresponding to that included in an IEEE 802.11 ATIM message) in its *hello* messages. Nodes wake up periodically and stay awake during a specified period of time, which is identified as the control and management (*C&M*) period. This period is selected in a manner that allows nodes to successfully send their most current *hello* message to their neighbors during the underlying period interval. Thus, any node that has a message to forward to a neighbor is able to notify and wake up this neighbor. Nodes that do not transmit or receive any wake up notification during the *C&M* period will sleep to conserve energy.

Nodes are synchronized to wake up at the beginning of each super frame. The time duration of a super frame is determined by the underlying multicast protocol. For our MBN power saving scheme, this is set to be 1 second. A frame synchronization mechanism is employed by the nodes. Accurate synchronization may be hard to achieve between nodes that are multi-hop away. However, we note that accurate frame synchronization acquisition is only required for the interaction between neighboring nodes. In [18], the authors proposes a synchronization mechanism for the operation in multi-hop networks, whereby the frequency at which synchronization beacons are generated is significantly reduced by requiring only nodes that are members of a minimum connected dominating set (MCDS) to send synchronization beacons. This approach is readily incorporated into our MBN power saving scheme.

Our MBN power saving scheme is specified in accordance with the finite state machine whose state transition diagram is shown in Fig. 2-7. A control and management (*C&M*) period is established at the start of each super frame, and it is equivalent to the ATIM interval in IEEE 802.11 power saving mode. While in this state, each node broadcasts a *hello* message to its neighboring nodes. A *C&M* timer is used for controlling the interval during which a node stays

in its *C&M* state. In our simulation, when a node has 20 neighbors, the size of its *hello* message is determined to be equal to 110 bytes. Thus, the transmission time of a *hello* message is equal to 0.44 ms, under a data rate of 2 Mbps. When the wireless link is not overloaded, our simulations have shown the overall MAC access delay to be (at the 99-percentile) lower than 1ms. We have adopted in our simulation a *hello* period duration of 50ms and this has proven to be sufficiently long for accommodating the *hello* message traffic load generated in our simulations under the prescribed nodal density.

Given that a node is in the *C&M* state, it will transition into the *active* state if any of following conditions is satisfied:

(i) The node has received wakeup notification(s).

(ii) The node is scheduled to send a data packet.

(iii)The node is elected to act as a backbone node (BN).

While in *active* state, a node can transmit and receive data packets. An *active* state timer is used for controlling the length of time that a node stays in *active* state. In our implementation, this *active* state duration is set to be 900ms. Note that a packet transmission that is not completed within an *active* state is continued during the subsequent *C&M* state.

A node transitions into *sleep* state to conserve energy when it is not engaged in any packet transmission or reception activity (to avoid the overhearing issue when the radio module of a node is in idle state). The duration in which a node stays in *sleep* state can be selected individually by each node. At the end of its *sleep* state duration, the node waits until the start of the subsequent *C&M* period and then transitions into *C&M* state. In our simulations, this *sleep* state duration is set to be 900ms.

Under our MBN power saving scheme, a node maintains a list of its neighboring nodes to which it needs to forward packets currently residing in its queue. A node uses this list to include wakeup notifications in its next *hello* message for the designated neighbors, and to ensure the availability of these neighbors

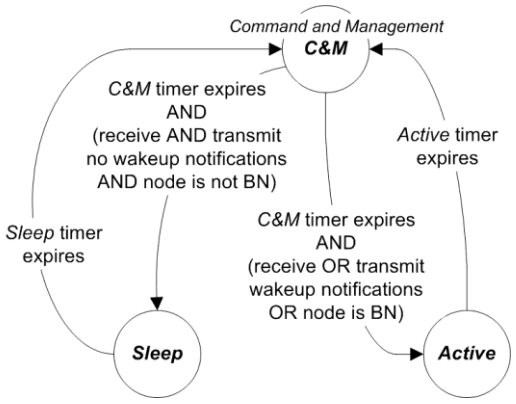

Fig. 2-7. Finite State Machine for the MBN Power Saving Scheme

B. ODMRP-Power Saving Scheme (ODMRP-PS)

On-Demand Multicast Routing Protocol (ODMRP) is a mesh-based multicast protocol that uses the forwarding group concept to select, for each multicast group a limited set of nodes for forwarding multicast messages. A Join-Query packet is periodically broadcasted to update the election of forwarding group members and refresh the end-user group membership information. For each multicast group, every source will construct a source-based shortest path tree (SPT) connecting to all of its designated group members. The superposition of these SPTs (of the same multicast group) will form the multicast forwarding mesh for ODMRP.

We modified the original ODMRP scheme to include a power saving mechanism for fair comparison with our MBN based multicast protocols. The state transition diagram of the finite state machine for ODMRP with power saving mechanism (ODMRP-PS) is shown in Fig. 2-8.

Although the exchange of *hello* messages is not required for ODMRP-PS, nodes are still required to synchronize to wake up at the beginning of each super frame. Note that the period of

the super frame is equivalent to the refresh interval of ODMRP. Again, frame synchronization mechanism is employed by the nodes, with accurate frame synchronization acquisition only required for the interaction between neighboring nodes as specified for the MBN power saving scheme. In the original protocol, Join Query messages are piggybacked in data packets and flooded across the whole network as part of the operation that constructs the multicast forwarding mesh. In our implementation, we decoupled the control and data forwarding mechanism of ODMRP to make the protocol more scalable, since the flooding of a relatively big data packets is undesirable. The decoupling also ensures a shorter interval for the sources to obtain Join Replies back from the receivers (the Query-and-Reply phase is performed in the *C&M* state), since the control packets have higher priority and data transmissions are deferred to be performed in the *active* state. However, the *C&M* period duration will depend on the size of network since it has to accommodate the round-trip time of the Query-and-Reply packets.

Once the Query-and-Reply phase is finished in the *C&M* state, a forwarding mesh is constructed. The selected forwarding nodes will transition into *active* state since they are responsible for data transmissions, while the non-forwarding nodes will transition into *sleep* state to conserve energy. In other words, the wakeup notifications for ODMRP-PS are embedded in the Query-and-Reply phase. The Forwarding-Group-Timeout feature of the original ODMRP scheme is still retained in our new implementation.

In our simulation, the time duration of a super frame for ODMRP-PS is set to be equal to its refresh interval (which in this case is 3 seconds). We have set the *C&M* period interval to be 300ms and this has proven to be sufficiently long for accommodating the round-trip time required by the Query-and-Reply phase for the underlying simulation network size and conditions, whereas the *sleep* and *active* state durations are both set to be 2.7 seconds.

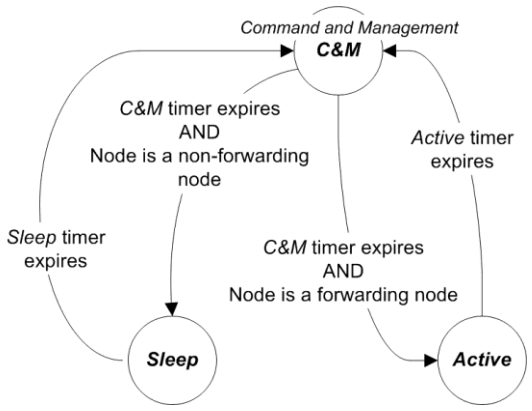

Fig. 2-8. Finite State Machine for the ODMRP-PS Scheme

2.7 References

[1] C. Wu and Y. Tay, "AMRIS: A multicast protocol for ad hoc wireless networks," in *Proc. of IEEE MILCOM*, 1999.

[2] S.-J. Lee, W. Su, and M. Gerla, "On-demand multicast routing protocol in multihop wireless mobile networks," *ACM/Baltzer Mobile Networks and Applications*, 2000.

[3] E. L. Madruga and J. J. Garcia-Luna-Aceves, "Scalable multicasting: the core-assisted mesh protocol," *ACM Mobile Networks and Applications,* Vol. 6, No. 2, pp. 151–165, 2001.

[4] J. Xie, R. R. Talpade, A. Mcauley, and M. Liu, "AMRoute: ad hoc multicast routing protocol," *Mobile Networks and Applications*, Vol. 7, No. 6, pp. 429–439, 2002.

[5] S.-J. Lee, W. Su, J. Hsu, M. Gerla, and R. Bagrodia, "A performance comparison study of ad hoc wireless multicast protocols," *Proceedings of INFOCOM 2000*, pp. 565–574, 2000.

[6] I. Rubin, A. Behzad, H. Ju, R. Zhang, X. Huang, Y.-C. Liu, R. Khalaf, "Ad hoc wireless networks with mobile backbones," *in Proc. of IEEE International Symposium on Personal, Indoor and Radio Communications (PIMRC)*, Vol.1, pp. 566–573, 2004.

[7] C. Tan and I. Rubin, "Multicasting in mobile backbone based ad hoc wireless networks," in *Proc. of IEEE WCNC*, 2006.

[8] S.-Y. Ni, Y.-C. Tseng, Y.-S. Chen, and J.-P. Sheu, "The broadcast storm problem in a mobile ad hoc network," in *Proc. of the 5th annual ACM/IEEE international conference on Mobile computing and networking*, pp. 151–162, 1999.

[9] X. Huang and I. Rubin, "Mobile backbone network routing with flow control and distance awareness," *in Proc. of IEEE MILCOM*, 2005.

[10] H. Ju and I. Rubin, "Performance analysis and enhancement for backbone based wireless mobile ad hoc networks," *in Proceedings of IEEE BroadNets*, pp. 789–798, 2005.

[11] W. Liang, "Approximate minimum-energy multicasting in wireless ad hoc networks," *IEEE Transactions on Mobile Computing*, Vol. 5, No. 4, April 2006.

[12] J. Wieselthier, G. Nguyen, and A. Ephremides, "On the construction of energy-efficient broadcast and multicast trees in wireless networks," *in Proc. of IEEE Infocom*, pp. 585–594, 2000.

[13] M. Maleki and M. Pedram**,** "Lifetime-aware multicast routing in wireless ad hoc networks," *in Proc. of IEEE WCNC*, 2004.

[14] P. Floreen, P. Kaski, et al. "Lifetime maximization for multicasting in energy-constrained wireless networks*," IEEE Journal on Selected Areas in Communications*, Vol. 23, No. 1, January 2005.

[15] L. Feeney and M. Nilsson, "Investigating the energy consumption of a wireless network interface in an ad hoc networking environment," *in Proc. of IEEE Infocom*, pp. 1548–1557, 2001.

[16] C. Gui, P. Mohapatra, "Efficient overlay multicast for mobile ad hoc networks," *IEEE WCNC'03*, 2003.

[17] J. Boleng, "Exploiting location information and enabling adaptive mobile ad hoc network protocols," *PhD Thesis*, Colorado School of Mines, 2002.

[18] G. Cao and J. L. Welch, "Accurate multihop clock synchronization in mobile ad hoc networks," *in Proc. of International Conference on Parallel Processing Workshop*, pp. 13–20, 2004.

[19] C. Jaikaeo and C. Shen, "Adaptive backbone-based multicast for ad hoc networks," *in Proc. of IEEE International Conference on Communications,* pp. 3149- 3155 vol.5, 2002.

[20] C. Gui and P. Mohapatra, "Scalable multicasting in mobile ad hoc networks", *in Proc. of IEEE INFOCOM*, pp.2119-2129 vol.3, 2004.

3 Joint Scheduling and Power Control for Multicasting in Cellular Wireless Networks

Efficient multicasting of messages in multimedia cellular networks to identified multicast group clients is a task of primary importance. Consider a wireless cellular network that consists of base stations that are interconnected through a backbone network, such as a LTE system as shown in Fig. 3-1. Messages targeted for multicast distribution are delivered across the backbone by content providers to base stations with clients that belong to the underlying multicast group. In this chapter, we study the coordinated adaptive-power scheduling of transmissions of such multicast packets by area base stations. The developed schemes are used by neighboring base stations to time-share their downlink channels over a prescribed frequency band. For application to LTE systems, such an operation is supported by the Multimedia Broadcast and Multicast Service (MBMS) [1],[2]. Our scheduling schemes are also highly effective when applied to meshed WiFi networks, or to mobile backbone based ad hoc wireless networks, whereby the roles of base stations are undertaken by access points or backbone nodes, respectively.

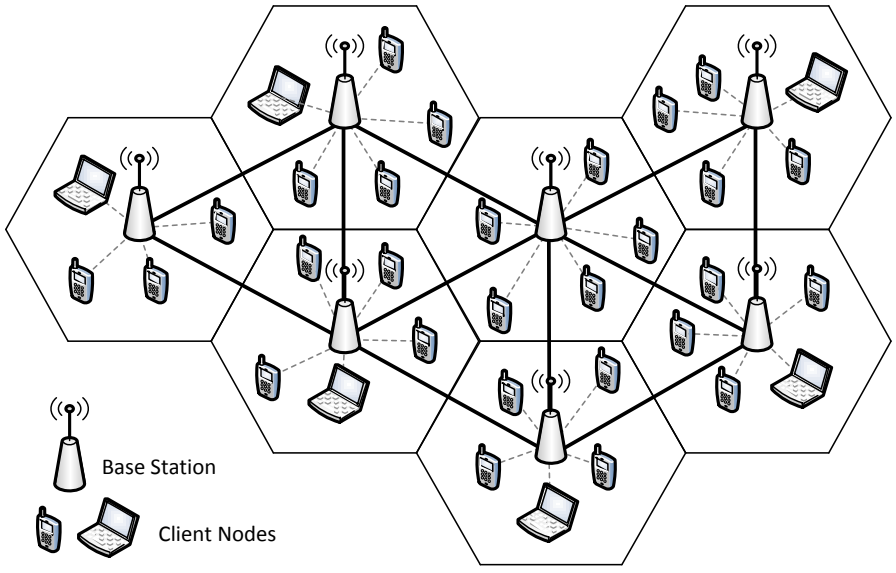

Fig. 3-1: Illustrative cellular system managed by backbone base stations

Under LTE MBMS, neighboring base stations may engage in coordinated time-synchronized point-to-multipoint transmissions. Client nodes may realize macro-diversity gains through selective combining or soft combining [2],[3]. Under a selective combining scheme used by MBMS over Single Frequency Network (MBSFN), multiple MBMS group base stations may be scheduled to transmit the same message at the same time, at the same rate, using the same modulation/coding scheme (MCS), to produce MIMO-type gains at receiving client nodes. Such an MBSFN operation requires strict time synchronization among base stations, thus imposing spatial configuration limitations, and increasing implementation complexity and costs [2],[4],[5]. In addition to combining operations, coordinated scheduling operations can also be performed across neighboring cells to manage inter-cell interference [6],[7].

In avoiding the use of such combining operations, the scheduling mechanisms developed here ensure each multicast transmission to be successfully received by all identified client nodes at targeted error rates, and thus at acceptable signal-to-interference-and-noise ratio (SINR) levels. Using the algorithms developed over LTE MBMS implementations, point-to-multipoint transmissions can be carried out by base stations, in a time coordinated fashion, across shared (OFDM-based) downlink channels, rather than using the MBSFN downlink structure. Such an implementation offers the following advantages:

(i) Different cells may contain different mixes of multicast client groupings. Thus, a base station that does not have clients that belong to a certain multicast group would not be configured to multicast (at the same time slot) packets that belong to this group for the sole purpose of achieving combining gains at client nodes of nearby base stations. This reduces energy consumption and increases spectral utilization efficiency.

(ii) Client nodes are not required to engage in MIMO-type (multipath combining oriented) operations, enabling the efficient operation of smaller user equipment, such as sensors and handheld smart phone platforms.

A wide range of schemes have been proposed to find the optimal link scheduling with power control for unicasting in spatial-TDMA networks [8]-[10]. Adaptive power control has been utilized by energy-aware multicasting schemes to synthesize a multicast structure that minimizes the total energy cost [11],[12]. However, to the best of our knowledge, we have found no published papers that solve the scheduling problem jointly with adaptive power control for multicasting in wireless cellular networks, under which base stations share their downlink channels on a coordinated spatial-TDMA basis.

The objective of this chapter is to develop efficient algorithms for such an operation and investigate the extent of throughput enhancement that can be feasibly attained. We first model the problem as a mixed-integer linear programming problem, use it to find an optimal solution, and conclude that the problem is NP-hard. We then present three computationally efficient heuristic algorithms that jointly determine the multicast schedule, the underlying base station transmit power levels and the set of client nodes that are addressed by each transmitting base station in each time slot. Consequently, a scheduled base station can make effective use of its allocated time slots to successfully transmit any mix of unicast and multicast packets. For scheduling unicast traffic, time slots allocated to a base station do not need to be re-negotiated and re-configured (hence reducing the ensuing rate of control traffic) as long as its mobile client nodes continue to reside in the geographical region that is targeted for coverage during the allocated time period. The presented algorithms can be readily extended to operations under

which base stations use sectorized antennas. Each scheduled downlink transmission is then targeted to cover a sector zone, rather than a disk-shaped geographical region.

The chapter is organized as follows. The system model is presented in Section 3.1. In Section 3.2, we model the joint scheduling and power control problem as a mixed integer linear program. We present our heuristic algorithms in Section 3.3. In Section 3.4, we study the performance of the system under our heuristic algorithms, as well as compare with that exhibited under the optimal solution. We also assess the spectral efficiency of our schemes in comparison with the corresponding performance behavior of illustrative LTE MBSFN systems.

3.1 System Model

We consider a cellular wireless network that consists of base stations with omni-directional antennas. Client nodes located in a cell region communicate through the base station with which they associate. We assume that the transmissions of multicast packets are scheduled over a prescribed frequency band, using a fixed transmit rate achieved under a prescribed modulation/coding scheme (MCS). Neighboring base stations are time-slot synchronized. They share their downlink channels on a coordinated spatial-TDMA basis. The time-slot duration is assumed to be equal to the transmission time of a prescribed load of packets, incorporating a sufficiently long preamble that compensates for incurred propagation delays.

Under our centralized algorithm, a scheduling controller is used to allocate time slots to base stations for the transmission of multicast messages. The controller periodically collects channel quality information (CQI) from client nodes, and uses the data to form a channel gain matrix for each downlink channel. We assume here that such updates are executed at a sufficiently fast pace to be of relevance for the time period over which the underlying slot allocation operation is performed. During this period of time, we assume the locations of client nodes and the

corresponding downlink transmission gain values to be essentially static. Base station i is capable of adjusting its transmit power continuously in a given range $[0, P_{max}(i)]$, in a slot-by-slot fashion. For the special case in which all base stations are limited by the same maximum power level, we denote the latter as P_{max}. Further adaptations can be carried out through the dynamic setting of the MCS and its ensuing code rate to attain performance upgrade; however, the purpose is to determine the contributions made by the sole use of transmit power adaptations on the performance behavior of multicast scheduling mechanisms. Moreover, the setting of the data rate (based on the MCS configuration) in the multicasting scenario is dictated by constrains imposed by the critical nodes.

Assume that we have M base stations and N multicast client nodes (representing mobile end user stations) in the underlying network region. Client nodes are initially associated with one of the M base stations by selecting the one from which they receive a control signal at the highest power level. As the scheduling operation progresses, it may often be effective to link a client node located at the edge of a cell with a different base station for the purpose of receiving certain scheduled multicast transmissions, without necessarily changing its primary association (as performed by an MBSFN system, yet without using here the combining operations). These edge clients are then 'removed' from their respective initial associated base stations. This results in the affected base stations to only require serving clients with closer proximity to them, leading to SINR improvement. We identify such an assignment as a multicast linking (*m-linking*) operation.

For a unicast transmission scenario, a directed communication link l_{ij} is established from node i to node j if there exists a power level $P \in [0, P_{max}(i)]$, under which the SNR level measured at the receiver of node j exceeds a prescribed threshold level $\gamma(j)$; i.e.,

$$G_{ij} P / \eta \geq \gamma(j) \tag{3-1}$$

where G_{ij} denotes the propagation gain incurred during the transmission, and η is the thermal noise power monitored at node j (which, without loss of generality, is assumed to be the same for all nodes). Such a model is often identified as the SINR-based interference model [13]. The value of the threshold $\gamma(j)$ depends on the prescribed block link error rate (BLER), modulation/coding scheme and ensuing data rate (or spectral efficiency) used by node j [14]. We henceforth assume here that a specific modulation/coding scheme is employed, so that under a prescribed BLER level for the link terminating at receiver j, the corresponding minimum acceptable SINR level is denoted as $\gamma(j)$. To simplify our algorithmic schemes, we further assume there that $\gamma(j) = \gamma$ for each node j. Consequently, each scheduled base station will transmit its packets in its allocated slots at a prescribed data rate.

For a multicasting scenario, let N^{Tx} represents the set of base stations with multicast messages to distribute and N^{Rx} denotes the set of client nodes interested in the underlying multicast packets. Let $G = \left\{ G_{i_k j_k},\ i_k \in N^{Tx},\ j_k \in N^{Rx}(i_k) \right\}$ represents the propagation gain matrix and $N^{Rx}(i_k)$ denotes the subset of client nodes that is associated with base station i_k (BS-i_k). Let $i_k \to N^{Rx}(i_k)$ and $P_{i_k}^{(t)},\ P_{i_k}^{(t)} \in [0, P_{\max}(i_k)]$ represent a multicast transmission by BS-i_k that reaches the entire group of multicast client associated with this base station, and the corresponding transmit power level in time slot t, respectively. For a transmission scenario $S(t) = \{i_1 \to N^{Rx}(i_1), \cdots \qquad \vee^{Rx}(i_M)\}$ at time slot t to be feasible under the power vector $\bar{P}(t) = (P_{i_1}^{(t)}, ..., P_{i_M}^{(t)}),\ 0 \le P_{i_k}^{(t)} \le P_{\max}(i_k),\ k = 1, 2, ..., M$, a transmission by BS-$i_k$ must be received at each of its client node with an SINR level that is higher than a prescribed threshold. Hence, for each BS-i_k, considering all the multicast client nodes that are currently linked with it, we require:

$$G_{i_k j_k} P_{i_k}^{(t)} - \gamma(j_k) \sum_{\substack{z=1 \\ z \neq k}}^{M} G_{i_z j_k} P_{i_z}^{(t)} \geq \eta\, \gamma(j_k), \quad j_k \in N^{Rx}(i_k). \tag{3-2}$$

Fact 1: The power vector $\overline{P}^{AP}(t) = (P_{i_1}^{(AP,t)}, ..., P_{i_M}^{(AP,t)})$ that satisfies the system of linear inequalities (2) in its equality form, when it exists, is referred to as the apex solution. If $S(t)$ is a feasible transmission scenario under $\overline{P}^{AP}(t)$, then any other power vector $\overline{P}'(t)$ under which $S(t)$ is feasible would require at least as much power (i.e., $\overline{P}'(t) \geq \overline{P}^{AP}(t)$ component-wise). Based on Perron-Frobenious theorem [15],[16], it is shown that if a transmission scenario $S(t)$ is feasible, the apex solution of the corresponding system of linear inequalities is strongly Pareto Optimal with respect to $S(t)$. Thus, this is an energy efficient solution; the apex point yields a solution that employs the lowest power level for each base station.

Using adaptive power control jointly with scheduling, we aim to design a time frame with the shortest schedule length to reach all of the respective multicast clients. The solution specifies the schedule, identifying in each time slot the set of transmitting base stations, their transmit power levels and the set of client nodes that each base station aims to reach. Under the optimal schedule, we also strive, as a secondary consideration, to employ a power efficient solution.

3.2 Mixed Integer Linear Programming (MILP) Model

In this section, we develop and investigate a MILP formulation for the joint adaptive-power multicast scheduling problem. We assume that the initial associations between clients and their base stations are determined based on a prescribed routine, such as that noted above, under which a user associates with the base station whose signal is received at the highest power level. The input for the optimization model is the set of designated base stations with multicast messages to distribute (N^{Tx}), the sets of multicast clients with their associated BS-i_k ($N^{Rx}(i_k)$,

$i_k \in N^{Tx}$), the traffic matrix, the propagation gain matrix (G), maximum transmit power of each BS-i_k ($P_{\max}(i_k)$), minimum required received SINR ($\gamma(j_k)$), and thermal noise power levels impacting the receivers of client nodes (η). To determine the system's throughput capacity level attainable under the employed scheduling scheme, we assume the allocated multicasting period to include a sufficient number of time slots to accommodate the multicasting of the load targeted for this period, so that the required time frame duration is upper bounded by a finite duration $T_{\max}$. The decision variables for the optimization algorithm are $\{X_{i_k}^{(t)}\}$ and $\{P_{i_k}^{(t)}\}$, where the binary variable $X_{i_k}^{(t)}$ is defined as:

$$X_{i_k}^{(t)} = \begin{cases} 1, & \text{if time slot } t \text{ is allocated to BS } i_k \\ 0, & \text{otherwise} \end{cases}$$
$$P_{i_k}^{(t)} \in [0, P_{\max}(i_k)] \qquad i_k \in N^{Tx}, \ \ t = 1, 2, \cdots \tag{3-3}$$

Every solution of the scheduling problem is represented as (***X,P***). The set of quadratic constraint:

$$G_{i_k j_k} P_{i_k}^{(t)} - \gamma(j_k) \sum_{r \in N^{Tx} - \{i_k\}} G_{r j_k} P_r^{(t)} X_r^{(t)} - \eta\, \gamma(j_k) \geq \Phi \cdot (X_{i_k}^{(t)} - 1),$$
$$(i_k, j_k) \in \left\{ i_k \in N^{Tx}, j_k \in N^{Rx}(i_k) \right\}, \ \ t = 1, \cdots \tag{3-4}$$

where Φ is a sufficiently large positive number, imposes the SINR requirement for a base station multicast transmission at time slot t. Note that if no transmission by BS-i_k is scheduled to take place at time slot t ($X_{i_k}^{(t)} = 0$), the associated constraint becomes redundant. We next show that this scheduling problem can be modeled as the following MILP formulation:

$$\textit{Minimize} \quad Z(X, P) = \sum_{t=1}^{T_{\max}} \sum_{i_k \in N^{Tx}} \left(c_t X_{i_k}^{(t)} + \varepsilon P_{i_k}^{(t)} \right) \tag{3-5}$$

$$s.t. \quad G_{i_k j_k} P_{i_k}^{(t)} - \gamma(j_k) \sum_{r \in N^{Tx} - \{i_k\}} G_{r j_k} P_r^{(t)} - \eta\, \gamma(j_k) \geq \Phi \cdot (X_{i_k}^{(t)} - 1),$$
$$(i_k, j_k) \in \left\{ i_k \in N^{Tx}, j_k \in N^{Rx}(i_k) \right\}, \ \ t = 1, \cdots \tag{3-6}$$
$$0 \leq P_{i_k}^{(t)} \leq P_{\max}(i_k), \quad t = 1, 2, \cdots \qquad i_k \in N^{Tx} \tag{3-7}$$

$$X_{i_k}^{(t)} = 0 \text{ or } 1, \quad t = 1, 2, \cdots \qquad i_k \in N^{Tx}. \tag{3-8}$$

In Eq. (3-5), ε is a sufficiently small positive number, and c_t is a positive constants defined as

$$c_t = t.|N^{Tx}|.c_{t-1}, \quad t = 2, ..., T_{\max}, \quad c_1 = 1. \tag{3-9}$$

It can be seen that the constraints expressed by Eq. (3.4 – 3.6) guarantee that a multicast transmission by BS-i_k will reach all the multicast clients under its management. The coefficients $\{c_t\}$ are used to ensure that the length of the schedule corresponding to the optimal solution of the MILP formulation is minimal, whereas the positivity of ε ensures the strongly Pareto optimality of the optimal transmit power levels deduced from the optimum solution of the MILP formulation.

Lemma 1. Every MILP solution yields a feasible transmission scenario at each time slot.

Proof. Consider an arbitrary time slot t under a feasible solution (***X,P***) of the MILP formulation, where $X = \left\{ X_{i_k}^{(t)}, i_k \in N^{Tx}, t = 1, \ldots \right.$ and $P = \left\{ P_{i_k}^{(t)}, i_k \in N^{Tx}, t = 1, \ldots \right.$. Assume that $S(t) = \{i_1 \to N^{Rx}(i_1), \cdots \quad \forall N^{Rx}(i_M)\}$. We claim that transmission scenario $S(t)$, when driven by power vector $\overline{P}(t) = \left(P_{i_1}^{(t)}, ..., P_{i_M}^{(t)}\right)$, is feasible. For a transmission $i_k \to N^{Rx}(i_k)$ in $S(t)$, since $X_{i_k}^{(t)} = 1$, based on (6), we have:

$$G_{i_k j_k} P_{i_k}^{(t)} - \gamma(j_k) \sum_{r \in N^{Tx} - \{i_k\}} G_{r j_k} P_r^{(t)} - \eta\, \gamma(j_k) \geq 0, \quad (i_k, j_k) \in \left\{ i_k \in N^{Tx}, j_k \in N^{Rx}(i_k) \right\}. \tag{3-10}$$

Since $X(t) \subseteq N^{Tx}$, we have:

$$\sum_{r \in N^{Tx} - \{i_k\}} G_{r j_k} P_r^{(t)} \geq \sum_{r \in X(t) - \{i_k\}} G_{r j_k} P_r^{(t)} = \sum_{\substack{z=1 \\ z \neq k}}^{M} G_{i_z j_k} P_{i_z}^{(t)}, \quad (i_k, j_k) \in \left\{ i_k \in N^{Tx}, j_k \in N^{Rx}(i_k) \right\}, \tag{3-11}$$

resulting in

$$G_{i_k j_k} P_{i_k}^{(t)} - \gamma(j_k) \sum_{\substack{z=1 \\ z \neq k}}^{M} G_{i_z j_k} P_{i_z}^{(t)} \geq \eta\, \gamma(j_k), \quad (i_k, j_k) \in \left\{ i_k \in N^{Tx},\, j_k \in N^{Rx}(i_k) \right\}, \tag{3-12}$$

which along with Eq. (3-7) confirms the feasibility of each transmission in $S(t)$. Consequently, transmission scenario $S(t)$ is feasible under power vector $\overline{P}(t)$. QED

The joint power control and scheduling problem for unicast transmissions, as presented in [9], can be reduced to an edge coloring problem, which is NP-hard [17]. Adding in the multicast nature of our problem, which induces further complexity since a single base station transmission has to satisfy the minimum SINR requirement imposed for each one of its multicast clients, implies that the underlying scheduling problem is also NP-hard. We therefore conclude the need for developing heuristic algorithms to provide solution schemes to this adaptive-power scheduling problem that is computationally efficient and scalable, when considering networks that may include a large number of base stations and client nodes.

3.3 Heuristic Algorithms for the Joint Power Control Scheduling Problem

We first introduce the notion of a Power Control Multicast Interference Graph [9], which is used as the basic building block for our heuristic Algorithm 1. Consider a scenario with only two base stations, BS-i_1 and BS-i_2, with corresponding sets of multicast clients $N^{Rx}(i_1)$ and $N^{Rx}(i_2)$. The transmission scenario $S(t) = \{i_1 \rightarrow N^{Rx}(i_1), i_2 \rightarrow N^{Rx}(i_2)\}$ is feasible if and only if the coordinates of the apex power vector solution of the following linear inequalities are in the range $(0,0) \leq \left(P_{i_1}^{(t)}, P_{i_2}^{(t)}\right) \leq \left(P_{\max}(i_1), P_{\max}(i_2)\right)$:

$$\begin{cases} G_{i_1 j_1} P_{i_1}^{(t)} - \gamma(j_1) G_{i_2 j_1} P_{i_2}^{(t)} \geq \eta\, \gamma(j_1) \\ -\gamma(j_2) G_{i_1 j_2} P_{i_1}^{(t)} + G_{i_2 j_2} P_{i_2}^{(t)} \geq \eta\, \gamma(j_2) \end{cases}, \quad j_1 \in N^{Rx}(i_1), \quad j_2 \in N^{Rx}(i_2). \tag{3-13}$$

To reduce the computational complexity of Eq. (3-13), we employ an approximation technique. Instead of inspecting the SINR condition for all multicast clients at each base station,

we consider for each pair of such base stations a pair of critical client nodes, one such node in each cell, whereby these nodes are located in positions that are estimated to be the most interference-prone locations (relative to the interference signals that are generated when only these two base stations are operational at the same time slot). We denote these critical receivers for BS-i_1 and BS-i_2 as j_1^* and j_2^*, respectively. Client nodes monitor their received interference power levels and report them to their base stations periodically via CQI updates. Base stations can then use this data to identify and select the critical client nodes. Assume transmissions $i_1 \to j_1^*$ and $i_2 \to j_2^*$ are the only two active transmissions in the network. The conditions stated in Eq. (3-13) are simplified to yield:

$$\begin{cases} G_{i_1 j_1^*} P_{i_1}^{(t)} - \gamma(j_1^*) G_{i_2 j_1^*} P_{i_2}^{(t)} \geq \eta\ \gamma(j_1^*) \\ -\gamma(j_2^*) G_{i_1 j_2^*} P_{i_1}^{(t)} + G_{i_2 j_2^*} P_{i_2}^{(t)} \geq \eta\ \gamma(j_2^*) \end{cases} \tag{3-14}$$

under a power vector $(0,0) \leq \left(P_{i_1}^{(t)}, P_{i_2}^{(t)}\right) \leq \left(P_{\max}(i_1), P_{\max}(i_2)\right)$. Thus, the approximation in (3-14) reduces the complexity of finding the apex power vector solution by considering all the multicast nodes between the 2 base stations under consideration to only the 2 critical nodes (one for each of the base station), and it is used in all of our numerical computations and simulations.

The multicast interference graph is defined as an undirected graph $U = (V, E)$ whose sets of vertices V and set of edges E are defined as follows. A vertex v_k in graph V represents a candidate multicast transmission from BS-i_k to its set of associated client nodes. Vertices v_1 and v_2 in V are connected to each other by an edge (which thus becomes an element of E) if and only if under which multicast transmissions by BS-i_1 and BS-i_2 cannot be executed during the same time slot, i.e., there is no feasible transmit power vector (P_{i_1}, P_{i_2}). The latter can be established by using Eq. (3-14).

3.3.1 Centralized Algorithm 1: Interference Graph Multicast Scheduling

Based on the constructed multicast interference graph, we introduce in this section a centralized heuristic algorithm that solves the problem in a polynomial efficient manner. It is an iterative scheme that consists of the following steps.

1. Every client node initially associates with a single base station based on the highest received power level.
2. We construct a multicast interference graph $U = (V, E)$ by considering only those base stations that have outstanding multicast packets to be scheduled, with each vertex representing a multicast transmission by a base station to its presently determined clients.
3. A maximum weight independent set of vertices of the multicast interference graph is selected. We set the weight of vertex v, $w(v) = h(v)/(d_U(v) + 1)$ where $h(v)$ denotes the density of the (as yet uncovered) client nodes of multicast transmission v, expressing the number of such mobile stations per unit area that are designated to receive multicast packet transmission from base station v, whereas $d_U(v)$ is the degree of vertex v in the graph U. An efficient greedy heuristic algorithm [18] is employed to obtain a maximal weighted independence set (i.e., transmission scenario) for the interference graph. In each iteration of the algorithm, one vertex is selected from the graph for inclusion into the weighted independent set. Vertex v is selected if it has the highest weight:

$$h(v)/(d_U(v)+1) = \max_{u \in V(U)} \{h(u)/(d_U(u)+1)\}. \quad (3\text{-}15)$$

Then, the selected vertex and all its neighbors are removed from the graph. Since nodal degree is indicative of the level of interference imposed by a multicast transmission, the use of this weight function leads to the selection of the next transmission that covers a

large number of client nodes (per covered area) while attempting to limit the level of interference that it may cause.

4. The resulting maximal independent set defines a provisional set of transmissions to be scheduled at this time slot. By definition of the interference graph, every subset of a maximal independent set with cardinality of two is a feasible transmission scenario. However, considering the accumulative effect of interferences, the entire maximal independent set does not necessarily form a feasible transmission scenario. The algorithm verifies the feasibility of the derived maximal independent set by checking the SINR level measured at each scheduled client node. For this purpose, we solve the set of linear equations that correspond to the set of Eq. (3-2) in its equality form, where candidate transmissions are members of the selected independent set. If this set is feasible, there exists a Pareto optimal solution, and the resulting power vector is used to set the transmit power levels of each scheduled base station in the independent set. If no such solution can be obtained, the selected independent set is determined to not be feasible, and we proceed with a pruning process by first removing the vertex that causes the most interference to other vertices in the graph [19]. The pruning procedure is repeated until the resulting transmission scenario is determined to be feasible.
5. The feasible transmission scenario generated from the previous pruning process is not necessarily maximal with respect to the underlying residual interference graph. To assure its maximality, we iteratively consider other remaining transmissions for possible addition to the currently selected feasible transmission set (see [9],[19] for details).
6. For each vertex selected as a member of the independent set, if the *m-linking* process is invoked, we determine if there are additional client nodes that can be covered by the

multicast transmissions executed by the corresponding scheduled base station. If so, the identified client nodes are now directed to receive multicast transmissions issued by this base station. Subsequently, the weights of vertices in the current residual interference graph are updated, taking these *m-linking* actions into account. This concludes the scheduling for the current time slot.

If there are still base stations with outstanding multicast packets, a new residual interference graph is formed by removing the vertices that have already been scheduled and have no more outstanding packets to be multicasted. The scheduling for such residual base stations proceeds to the next time slot by repeating steps 3-6 over the residual graph. This process is terminated when the multicast load of all the base stations are scheduled.

3.3.2 Centralized Algorithm 2: Maximal Simultaneous Multicast Transmissions

In this section, we introduce our second centralized heuristic algorithm. For each time-slot t, the algorithm constructs a feasible transmission set by iteratively scheduling additional multicast transmissions until no more such transmissions can be included. In each iteration, the algorithm attaches a weight metric β to every base station that has transmissions that are yet to be scheduled. The base station with the current highest β value is then evaluated. It is added to the set of base stations scheduled for transmission in this time slot if the newly expanded schedule is determined to be feasible. Otherwise, the base station with the next highest β value is considered. Base stations with outstanding multicast packets to be scheduled will remain on the residual base station list (set of base stations that are yet to be scheduled). Clearly, a fairness oriented or priority based mechanism can be readily incorporated to manage the order at which multicast transmission requests are queued at the scheduler, when the capacity (or time period) allocated for multicasting purposes is limited. Such considerations are not included. The iteration process

for time slot t is terminated when no additional base stations can be appended. Subsequently, the scheduling process continues in the same fashion at the next time slot.

The weight metric $\beta(i)$, calculated by BS-i is defined as $\beta(i) = \text{ratio}(i) \times \Delta_{\max}(i) / P_{\min}(i)$, where ratio($i$) is the number of clients associated with the examined BS-i, divided by the total number of clients that are associated with all residual base stations. We set $\Delta_{\max}(i)$, when determined to be non-negative, to represent the current power margin level at BS-i. It is defined as $\Delta_{\max}(i) = P'_{\max}(i) - P_{\min}(i)$, where $P'_{\max}(i)$ represents the maximal transmit power that can be used by BS-i while yielding a currently feasible operation; i.e., without degrading the received SINR values incurred at already scheduled client nodes to levels that are lower than their acceptable SINR levels. The parameter $P_{\min}(i)$ denotes the minimal transmit power that BS-i must utilize to reach its targetted client nodes at acceptable SINR levels. Each base station uses CQI data that it periodically receives from its client nodes to calculate the gain matrices for its associated downlink channels and to compute the interference power margins available at its critical client nodes [3],[20]. Base stations exchange such information, or pass it to the central scheduling controller, as well as identify the locations of their critical users (so that the channel gains for transmissions from a base station to critical nodes in neighboring cells can be estimated). The controller, and possibly also each base station, is then able to compute the above mentioned three key parameters and derive its weight metric.

In motivating the setting of the β weight metric, we note the following. In selecting the next multicast transmission to add to the schedule, we provide preference to base stations that serve a higher number of clients. We also prefer to select base stations that exhibit a higher transmit power margin level, since this would potentially realize a higher spatial reuse factor. In addition, we attach higher weights to base stations that require lower minimum power levels; consequently

tending to cause a lower level of interference to other transmissions. The steps of the algorithm are described as follows:

1. As used in Algorithm 1, every client node initially associates with a single base station based on the highest received power level.
2. The algorithm starts by determining the schedule and power levels for those base stations selected to operate in the first time slot. It continues in the same manner for scheduling outstanding multicast transmissions, if any, for subsequent time slots. At each time slot t, the process proceeds in an iterative manner, whereby the selection of the (k-1)-st addition of a base station to the transmission schedule is followed by considering the residual base stations and selecting, when feasible, the k-th addition of a base station to the schedule.
3. Initially, and at the end of each iteration step at which a new base station has been added to the schedule, each client node scheduled for reception at this time slot updates its CQI and sends the update to its base station. The latter then computes the level of additional interference at its critical nodes that can be still incurred, identified as the current marginal interference power level, and sends this information to the controller.
4. Based on data made available to base stations at the termination of step k-1, each residual BS-i calculates the weight metric $\beta(i)$ at step k by using the updated parameters ratio(i), $P_{\min}(i)$ and $P'_{\max}(i)$. The latter three parameters are calculated as follows:
    a. The ratio(i) is computed by the controller using the data received from BS-i that identifies the number of its current uncovered multicast clients. The value of ratio(i) is impacted by the *m-linking* process employed at previous iterations, when invoked.

b. The minimum power level $P_{\min}(i)$ at which BS-i must operate to successfully cover its multicast clients is calculated by the controller (on behalf of BS-i), or by BS-i itself, utilizing the marginal interference power levels reported from the critical client nodes and the latest downlink channel gain values of BS-i.

c. The calculation of the parameter $P'_{\max}(i)$ at the start of iteration k is also based on the collected CQI data, interference margins and channel gain matrices, updated at the conclusion of iteration k-1. The controller calculates for each residual BS-i, the maximal transmit power $P'_{\max}(i)$ at which it can operate, assuring acceptable SINR levels at critical client nodes that have already been scheduled.

5. Using the calculated $\beta(i)$ values, only base stations with positive $\Delta_{\max}(i)$ levels are considered. For each candidate BS-i, we set its transmit power level (if selected) to be $P(i) = P_{\min}(i) + \Delta(i) \le P'_{\max}(i)$, whereby $\Delta(i)$, $0 < \Delta(i) \le \Delta_{\max}(i)$. It is noted that by setting a higher value of $\Delta(i)$ increases the residual margin at the receiver of node's i transmission, but at the same time lowers the residual interference margin at receivers that have already been scheduled at this time. To simplify the implementation of the algorithm, we proceed to select the middle value for $\Delta(i)$ for the simulation results presented in the latter section

6. The base station with the highest weight metric β is then elected for addition to the schedule compiled (at this iteration k) for the current time slot t.

7. At the conclusion of iteration k, when a new base station is added to the schedule, we determine whether its multicast transmission can be effectively received by client nodes that are currently not associated with it. If such clients are identified, we proceed with the

m-linking process, when invoked, by directing these clients to receive the underlying multicast transmissions during this time slot from the newly selected base station.

8. This process is repeated until no additional base stations can be included in the schedule. If there are still base stations with outstanding multicast packets, the process of scheduling such residual stations is repeated by proceeding to the next time slot.

3.3.3 Distributed Algorithm 3

A distributed heuristic algorithm is developed by implementing the approach described for Algorithm 2. Each BS-i calculates a weight metric $\varphi(i)$ that is similar to the weight metric used in Algorithm 2. It is defined as $\varphi(i) = n_c(i) \times \Delta(i) / P_{\min}(i)$, where $n_c(i)$ is equal to the current number of clients associated with BS-i, $\Delta(i)$ represents the current power margin level for BS-i, and $P_{\min}(i)$ is the current minimum transmit power that is computed for BS-i. Each base station BS-i includes its current weight metric $\varphi(i)$ in control packets that it periodically distributes to its neighboring base stations that are within h hops from itself. Through this mechanism, base stations gather metric level data for their h-hop neighborhood (also identified here as BS-neighborhood), where $h > 0$. The value of h is selected to allow two base stations that are located at a distance of at least h+1 hops from each other to engage in simultaneous transmissions when using their maximum transmit power levels. For example, when operating under the parameters configured for our simulation scenario (refer to Section 3.4), it is generally sufficient to set $h = 2$.

During each scheduling iteration step, at each available time slot, the base station with the highest weight φ in its h-hop BS-neighborhood elects itself as a candidate for inclusion in the current schedule. The transmit power levels to be used by such candidates are determined using calculations noted below. If these computations lead to a feasible solution, the contending multicast transmissions of the winning base stations are then added to the set of scheduled

multicast transmissions. Such an election mechanism leads to a self-selection outcome under which two winning base stations (at a given time slot) must be h+1 hops away from each other. The scheduling process proceeds in this fashion until, in all BS-neighborhoods, no more base stations can add themselves to the schedule at the current time slot. The process is then repeated by residual base stations for the subsequent time slot. Steps of the algorithm are described below.

1. Base stations periodically transmit test signals at their maximum power levels. A preliminary association of multicast clients with a base station is performed based on the base station from which it has received the strongest signal.
2. Initially, and at the end of each iteration step, each residual base station updates its collected CQI data, interference power margins and channel gain matrices and computes the marginal interference power level for its critical client nodes.
3. At the start of each iteration in each time slot, each residual base station BS-i calculates its weight metric $\varphi(i)$. The base station includes the value of this parameter in control packets that it periodically distributes in its h-hop BS-neighborhood. The parameter n_c(i) is compiled by BS-i by counting the number of its current client nodes, whereas $P_{\min}(i)$ and $P'_{\max}(i)$ are calculated by BS-i using the same procedures described in Algorithm 2. Once a scheduling assignment is made and tested, if the received SINR levels are determined to be acceptable, each critical client node notifies its base station as to the interference margin level that it can still sustain. The base station distributes this data in its BS-neighborhood. If this margin level is close to zero, no further multicast transmissions that impact this critical client node can be allocated at this time slot.
4. As used for Algorithm 2, each candidate BS-i sets its transmit power level (if selected) to be $P(i) = P_{\min}(i) + \Delta(i) \le P'_{\max}(i)$, whereby $\Delta(i)$, $0 < \Delta(i) \le \Delta_{\max}(i)$.

5. As performed in Algorithm 2, when *m-linking* is invoked, the value of $n_c(i)$ is modified by allowing the effective current number of users served by certain base stations to be updated. Subsequently, BS-*i* updates its $\varphi(i)$ weight metric.
6. The BS-*i* that has announced the highest φ value in its *h*-hop BS-neighborhood elects itself for inclusion in the transmission schedule agreed upon for the current time slot. It is noted that base stations that belong to different BS-neighborhoods may elect themselves as candidates to join the schedule in a time slot. We assume time slots to be synchronized over the region of operation, so that, simultaneous transmissions by elected base stations over the same time slot can be executed.
7. A BS-*i* that has added itself to the schedule proceeds to transmit a test signal at power level $P'_{\max}(i)$. The client nodes that are the intended receivers of such multicasts measure the ensuing interference power and SINR levels. For this purpose, measurements may only be performed by critical client nodes. Client nodes that are located in other cells and have been scheduled to receive multicast transmissions at this time slot, inform their respective base stations about the acceptability of newly generated interference signals, if any. If the underlying SINR targets are met (as is expected to usually be the case), the current schedule is deemed feasible under the selected transmit power levels.

If the schedule is determined to not be feasible due to the measurement of unacceptable interference signal levels at client nodes that belong to the BS-neighborhood of BS-*i*, the latter base station deletes the addition of its latest transmission to the schedule. It announces this deletion in its BS-neighborhood, and terminates the process of contending for scheduling its transmission in this time slot. Base stations with outstanding load that are not impacted by such infeasibility events continue their scheduling process at the next iteration step. When all residual

base stations in a BS-neighborhood of a base station announce themselves to be in scheduling-termination state (i.e., they are not able to execute any additional transmissions at this time slot), the base station then continues the scheduling process by proceeding to the next time slot.

3.3.4 Computational Complexity

In the following section, we show that the computational complexity of our heuristic algorithms is of polynomial order. Assume there are M base stations and N client nodes in the network. Assume that each base station has B neighboring base stations and that C client nodes residing in each cell. Under our Centralized Algorithm 2, each base station calculates its weight level by computing the parameters ratio(i), $P_{\min}(i)$ and $P'_{\max}(i)$. For this purpose, each base station performs an order of (1+C+B) calculations. Each base station then compares its weight level with the weight values announced by other base stations, determining whether its weight level makes it a current winner. Such a determination involves (at most) M comparisons. The iterative process used to obtain the schedule for a single time slot can repeat at most M times. We note that the schedule (serving the given load) will be completed after a finite number K of time slots is assigned, noting that generally $K = O(M)$. Hence, the computational complexity of our Centralized Algorithm 2 is of the order of $O(M^3) + O(M^2(C + B))$.

For distributed algorithm 3, the analysis is similar except we note that during the contention phase, each contending base station compares its weight level only with those announced by base stations that are in its 2-hop neighborhood (which are of the order of $B^2 < M$). The number of iterative calculations executed in each time slot is of the order of B^2. These considerations lead to computational complexity of the order of $O(MB^4) + O(MB^2C)$. To ensure the realized SINR at intended receivers is acceptable, it is now required for each newly scheduled base station to transmit test signals and receive confirmation response messages from critical client nodes. The

computational complexity for this process increases when it is determined that the selected transmission is not feasible, since the recently scheduled base station must be dropped from the schedule and the contention phase must be re-run. At any rate, it is still of the order of the number of base stations residing in the 2-hop neighborhood, as used for the complexity bound noted above. However, the occurrence rate of such events is generally determined to be low, assuming that sufficient margin is allowed to account for the low impact caused by interference signals that originate by transmissions of scheduled base stations that are located outside the underlying 2-hop neighborhood.

We note that the computational complexity associated with Algorithm 1 is much higher than the corresponding levels for Algorithms 2 and 3. The controller proceeds first to construct an interference graph, which involves a number of comparisons of the order $O(M^2)$. To find an independent set, in each iteration of the process, a node with the highest weight is selected, which entails an order of M comparisons; this is iterated a number of times that is of the order of M; thus the process is then of the order $O(M^2)$. The controller then checks the feasibility of the derived schedule. Such a check is of $O(M^2)$, as it requires solving the set described by Eqs. (2), considering critical nodes (whose number is of the order of M). The pruning and supplemental subsequent stages are each of order $O(M^3)$.

Property 1. The iteration process employed by heuristic Algorithms 2 and 3 terminates after a finite number of steps with a feasible schedule.

Proof. Under both algorithms, for each iteration step in a time slot, each residual base station is capable of computing a unique weight metric. The election procedure yields a single winner with the highest metric in each contending neighborhood in which the winner is to be added to the schedule if it passes the feasibility test. The subsequent testing period allows client nodes to

measure the underlying SINR levels and report back to their base stations, affirming (or not) the feasibility of new transmission additions (in their cell or in neighborhood cells) to the schedule, and updating the underlying CQI data. It is noted that during each iteration step in a time slot, when the process has not been terminated, at least a single multicast transmission is scheduled in a neighborhood. The number of outstanding packets to be multicasted during the underlying period, which is finite, is therefore reduced during each such step. Furthermore, the addition of new transmissions to an existing schedule in each time slot is executed only if it guarantees the continued feasibility of existing transmissions, therefore avoiding assignment cycles.

For the distributed algorithm, it is possible for residual base stations that belong to distinct *h*-hop BS-neighborhoods to simultaneously engage in scheduling processes. As noted above, the employed interference margins assure the feasibility of simultaneous transmissions by base stations that belong to distinct BS-neighborhoods. We have assumed an area of operation with a finite number of base stations and thus neighborhoods, so that the complete scheduling process involves a finite number of steps and time slots. For the centralized algorithm, the controller can perform its scheduling of transmissions on a sequential slot-by-slot basis, so that the process clearly terminates after a finite number of iteration steps and time slots. QED

3.4 Performance Behavior

To study the performance of our algorithms, we have used MTALAB to simulate and analyze a homogeneous cellular network with 25 macro base station cells, with inter-site distance (ISD) of 1.732 km. The value of the ISD is selected such that the cell transmission radius is equivalent to $R = ISD/\sqrt{3} = 1000m.$ To demonstrate that our heuristic algorithms also yield efficient schedules under heterogeneity, we later consider a heterogeneous network layout that includes both macro and micro base stations. The micro base stations are placed between the

macro base stations and are thus used to cover edge clients of the macro cells, as shown in Fig. 3-2. We assume that a micro base station can adjust its transmit power level continuously in the range 0-10W, whereas a macro base station has an adjustable transmit power range of 0-40W. The channel propagation gain is modeled as $G_{ij} = K/d_{ij}^{\alpha}$, where d_{ij} is the distance between the transmitter and its receiver, and α denotes the path loss exponent. The constant K accounts for propagation losses, such as absorption and penetration losses. We have assumed in our simulations that $\alpha = 3.68$ and set $10\log(K)$ to be -40 dB, corresponding to a version of the urban Cost-Hata model used in LTE network studies [5],[21],[22]. For comparison purposes, we do not account for random fading components (which consists of mostly shadow fading variations for LTE downlink channels).

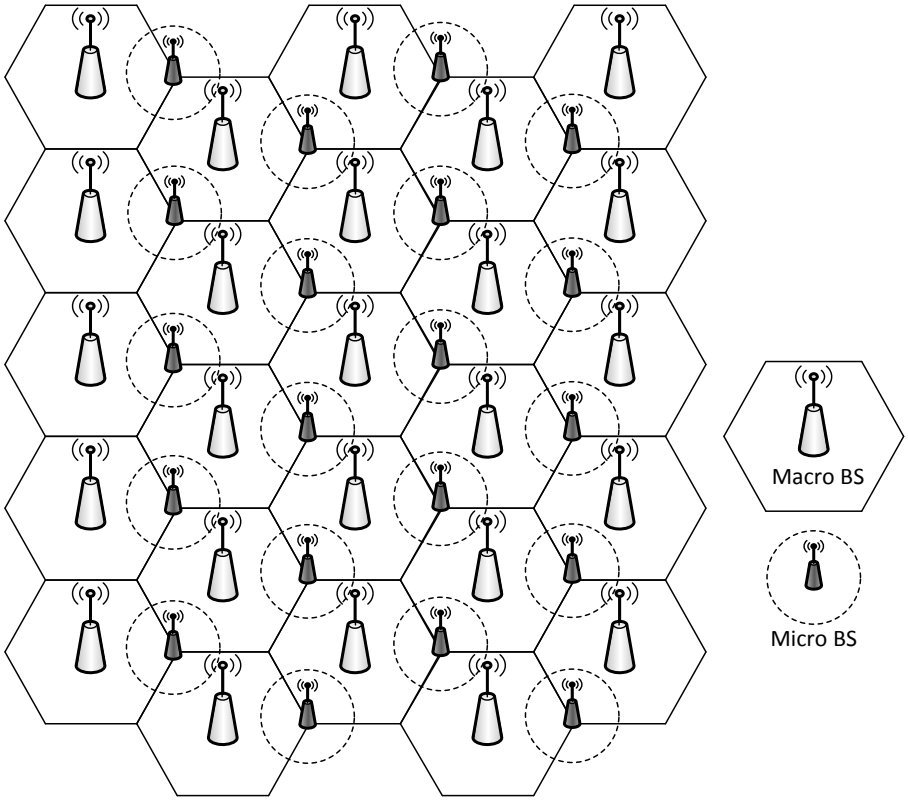

Fig. 3-2: Heterogeneous network grid layout using macro and micro base stations

In our simulation, we aim to provide coverage to all clients. The realized data rate utilization level (or spectral efficiency), denoted as ψ [bps/Hz], depends upon the implemented MCS. To compare with studies presented in the referenced papers that use a basic rate of 2 [bps/Hz], we set the minimum required SINR level for each client node in our study to be 4 dB. Under an additive white Gaussian noise type channel, this leads to a Shannon's capacity bound that yields $\psi \leq \log_2(1+\text{SINR}) = 2.32$ [bps/Hz]. The noise power density N_0 is set to be -174dBm/Hz, and the transmission bandwidth is set to 5 MHz. Client nodes are randomly distributed across the area of operation. The attained receive throughput rate is presented in units of [packets/slot/user], whereby the slot duration is set equal to the transmission time of a single packet. Thus, a throughput rate of 1 [packet/slot/user] represents a *receive* throughput rate of ψ [bps/Hz/user].

We first consider a homogeneous cellular network that consists of 25 macro base station cells. The performance results, depicted in Fig. 3-3, indicate that the centralized heuristic Algorithm 1, though having a much lower computational complexity, yields performance behavior that is only slightly degraded (around 10% - 15%) when compared with that exhibited by the MILP-based algorithm that yields the optimal schedule and transmit power setting. It is noted that the *m-linking* process has not been invoked for this comparison.

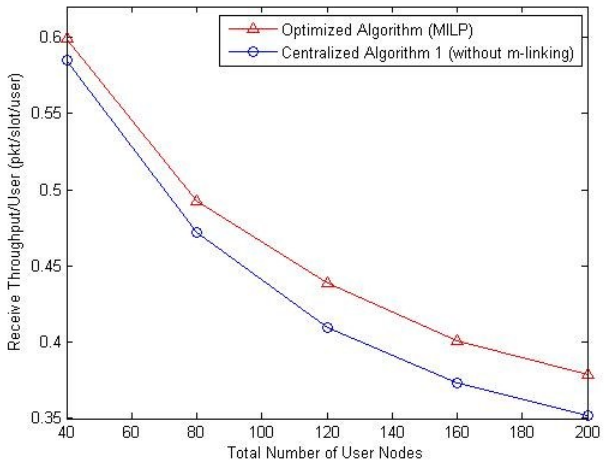

Fig. 3-3: Performance comparison between Optimized Algorithm and Centralized Algorithm 1, without the m-linking process

In Fig. 3-4, we compare the per-user receive throughput rate, as a function of the total number of multicast clients in the system, as attained by our algorithms. We observe that Algorithm 2 achieves a slightly lower throughput rate performance (by about 4% - 7%) than that attained under Algorithm 1, while Algorithm 3 exhibits a throughput rate that is further slightly degraded (by about 8% - 12%). We note that Algorithms 2 and 3 offer much reduced level of algorithmic computational complexity, and that Algorithm 3 entails a fully distributed implementation. For all three algorithms, we observe that as the number of clients over a prescribed area of coverage increases, an increasing number of time slots per frame is required. However, the corresponding reduction in per-user throughput rate attained under each algorithm becomes much less noticeable with further increases in client population. The synthesized schedules tend to more fully cover the complete geographical area of operation, so that multicast schedules performed to accommodate a larger number of clients will then more often also cover new clients.

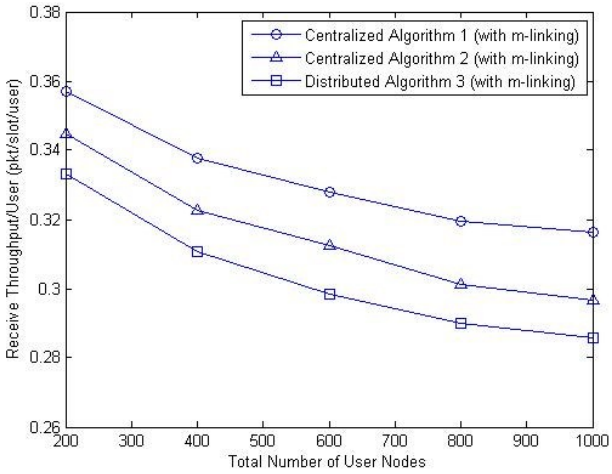

Fig. 3-4: Performance comparison between the heuristic scheduling algorithms

To assess the throughput gain attained by our adaptive power scheduling algorithms, when compared with LTE MBSFN schemes, we note the following. Assume that our multicasting scheme is used to share a prescribed LTE bandwidth segment, which consists of OFDM downlink channels, among neighboring base stations. Each symbol is transmitted across a narrow-band subcarrier, and is attached a cyclic preamble of sufficient length such that with the use of 1-tap equalization at the client receivers, no multipath fading interference is incurred [3]. Lognormal shadow fading effects can be readily included, but we neglect their effect in the following discussion since it does not impact our comparisons.

In assessing the performance behavior of OFDMA-based MBSFN systems, the study in [22] uses a bandwidth of 5MHz and an inter-site distance (ISD) of 1.732 km. To attain complete coverage of all client nodes (at a block link error rate of 10%), it is determined in [22] that the common MCS that must be used by all base stations corresponds to CQI 3, which maps to an SINR value of about -3 dB. The corresponding spectral efficiency is shown to be about 0.294 [bps/Hz]. Another MBSFN scheme presented in [5] assures a target coverage probability of 95%. Using an ISD of 1 km and a bandwidth of 5 MHz, it is shown that the best MCS to use for this

ISD level is 16 QAM 1/2. Using this MCS, the system is shown to attain a spectral efficiency of about 0.28 [bps/Hz], and thus a throughput rate of about 1.4 Mbps for multicasting over a single cell (see [5] Table III). In comparison, our "worst" performing Distributed Algorithm 3 achieves a throughput rate of about 0.28 - 0.33 [packets/slot/user], or 0.28ψ - 0.33ψ [bps/Hz/user]. When the system operation is associated with an MCS code rate with $\psi = 2$ [bps/Hz], such as 16 QAM 1/2, our scheme yields a throughput rate that is equal to about 0.56 - 0.66 [bps/Hz/user], leading to a data rate of 2.8 – 3.3 Mbps. This is higher than the spectral efficiency values of 0.28 [bps/Hz/user] and 0.294 [bps/Hz/user] achieved by [5] and [22], respectively.

By including the cyclic preamble overhead involved in OFDMA systems, the induced reduction in throughput rate is typically in the order of at most 5% - 10% ([5],[22]). For all schemes, further reduction in the realized spectral efficiency level is incurred when shadow fading is accounted for. Since the focus here is on the role of adaptive power operations alone, we have not included the potential enhancement achievable with data rate adaptations. We further note that under our algorithms, neighboring base stations are not required to employ the same MCS. We conclude that our algorithms achieve performance efficiency that is as high as, or higher than, that attained by the referenced LTE MBSFN operations that employ sophisticated MIMO-type signal combining techniques.

We next consider a system in which clients are divided into two multicast groups. We evaluate two multicast scheduling approaches. Under the first approach, multicast transmissions to each group are separately scheduled – in each time frame, two sequential time-division subframes are executed, i.e., transmissions to group 1 clients are scheduled in subframe 1, followed by transmissions to group 2 clients in subframe 2. Such an operation mimics the MIMO approach, under which the same packets are scheduled for transmission at the same time by

multiple base stations (though we employ no combining operations). In turn, under the second approach, multicast transmissions that belong to the two multicast group sessions are jointly scheduled. In this case, base stations that are scheduled to engage in transmissions in a certain time slot may use the allocated time slot to transmit packets that belong to any multicast group. For both cases, we have implemented the scheduling process by using Centralized Algorithm 2, incorporating the *m-linking* process. The performance results are displayed in Fig. 3-5. They show that the joint scheduling scheme leads to a higher per user throughput rate (by about 7% - 16% for cases under evaluation). As noted above, the joint scheduling operation provides much higher flexibility in accommodating transmissions of varying loading levels of multiple multicast group traffic flows. Such an operation is noted to lead to schedules that achieve higher spatial reuse factors, and therefore attain enhanced per user throughput rate performance behavior.

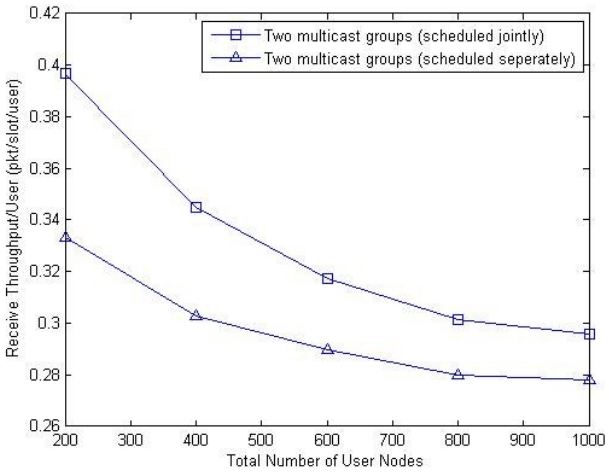

Fig. 3-5: Performance of the scheduling algorithm when multiple multicast groups are involved

To demonstrate the performance advantage that can be gained through the use of transmit power adaptations, we compare the performance of such adaptive-power algorithms with corresponding scheduling schemes that set the transmit power level of base stations to be fixed at their maximum specified levels. For both schemes, we utilize the scheduling mechanism

specified by distributed heuristic Algorithm 3. Performance results are shown in Fig. 3-6. We observe that by fixing the transmit power level, the scheduling scheme realizes a lower spatial reuse factor, requiring therefore a larger number of time slots to complete the execution of multicast transmissions, leading to reduced per user throughput rates by about 25% - 35% for the examined *m-linking* scenario. The results displayed in Fig. 3-6 also demonstrate the advantage gained through the *m-linking* process; this process is noted to improve the throughput rate for the power adaptation scenario by about 11% - 16%.

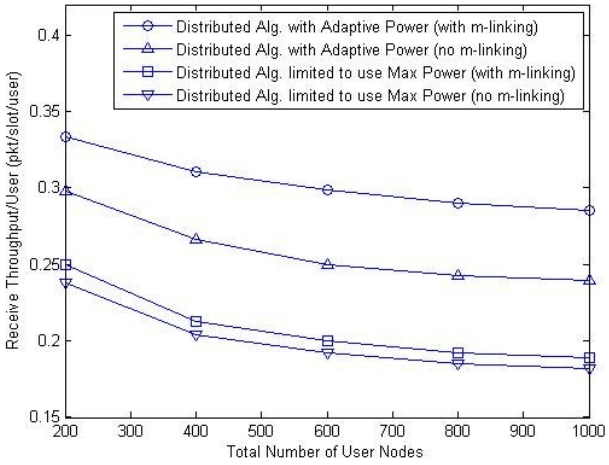

Fig. 3-6: Performance comparison between adaptive-power scheduling algorithms and those that use fixed base station transmit power levels

In Fig. 3-7(a), we compare the per user throughput rate performance behavior attained under the homogeneous and heterogeneous layouts. We observe that our adaptive-power scheduling algorithms also operate effectively under a heterogeneous layout. Furthermore, the latter layout is noted to lead to enhanced per-user receive throughput rates since our algorithms effectively use the micro base stations to cover their nearby clients. Under the homogeneous layout, the latter client nodes would reside in high interference cell-edge regions.

To assess the energy-based throughput performance gains that are achieved by our schemes, a performance measure that accounts for the total number of multicast bits transported by the system per unit energy expanded is used. The ratio of the corresponding measures attained for the corresponding fixed and adaptive power schemes, denoted as ζ is:

$$\zeta = \sum_{i=1}^{N}\sum_{j=1}^{N_{TS}^{\max}} P_i^{\max}(j) I_i^{\max}(j) \Bigg/ \sum_{i=1}^{N}\sum_{j=1}^{N_{TS}^{adapt}} P_i^{adapt}(j) I_i^{adapt}(j), \qquad (3\text{-}16)$$

where N_{TS}^{adapt} and $N_{TS}^{\max}$ represent the number of time slots required by the employed adaptive and fixed power schemes, respectively; $P_i^{adapt}(j)$ and $P_i^{max}(j)$ are the corresponding transmit power levels selected for BS-i when scheduled to transmit its multicast messages in time slot j, and the indicator function $I_i(j)$ is set to 1 if BS-i is assigned to transmit at time slot j, and is set to 0, otherwise. The sets $\{I_i^{adapt}(j)\}$ and $\{I_i^{max}(j)\}$ identify the schedule plans enacted under the adaptive and fixed power schemes, respectively.

In computing the ratio metric ζ involving the receive throughput rate per unit power, we observe in Fig. 3-7(b) that the adaptive power scheme, when applied to the homogeneous base station layout, achieves a receive throughout rate per unit power performance that is about 20% - 38% higher than that obtained under the fixed power scheduling scheme. An even better such energy aware performance metric is noted to be attained under the heterogeneous base station layout, yielding performance improvement factors of about 23% - 51% for the adaptive scheme. Thus, for the investigated simulation scenarios, the adaptive power scheduling scheme has been proven to derive schedules that yield high throughput rate and high throughput rate per unit power performance for homogeneous as well as heterogeneous base station layouts.

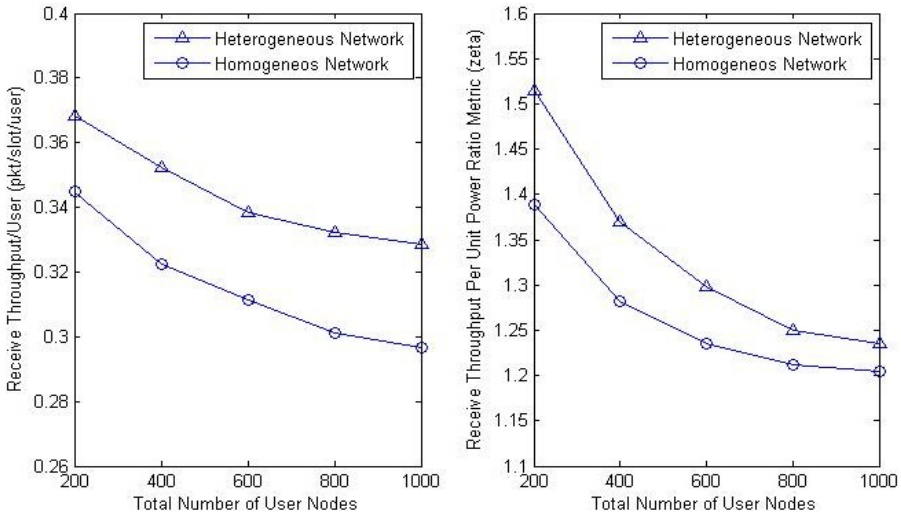

(a) (b)

Fig. 3-7: Performance comparison of the adaptive-power multicasting algorithms for homogeneous and heterogeneous cellular network layouts: (a) Per-user receive throughput rate (b) Throughput rate per unit expanded communications power ratio metric

3.5 References

[1] 3GPP TS 23.246 v. 9.3.0, "Technical Specification Group Services and Architecture; Multimedia Broadcast/Multicast Service (MBMS), Architecture and Functional Description," Rel. 9, 2009

[2] 3GPP TS 25.346 v. 9.1.0, "Technical Specification Group Radio Access Network; Introduction of the Multimedia Broadcast/Multicast Service (MBMS) in the Radio Access Network," Rel. 9, 2010

[3] F Khan, *LTE for 4G Mobile Broadband* (Cambridge University Press, 2009)

[4] A Alexiou, C Bouras, V Kokkinos, G Tsichritzis, "Communication cost analysis of MBSFN in LTE," in *Proceedings of the IEEE 21st International Symposium on Personal Indoor and Mobile Radio Communications*, pp. 1366-1371, 2010

[5] L Rong, O Ben Haddada, S-E Elayoubi, "Analytical analysis of the coverage of a MBSFN OFDMA network," in *Proceedings of the IEEE Global Telecommunications Conference*, pp. 1-5, 2008

[6] R Irmer, H Droste, P Marsch, M Grieger, G Fettweis, S Brueck, H Mayer, L Thiele, V Jungnickel, "Coordinated multipoint: concepts, performance, and field trial results," in *IEEE Communications Magazine*, vol. 49, no. 2, pp. 102-111, 2011

[7] P Marsch and G Fettweis, "On multi-cell cooperative transmission in backhaul-constrained cellular systems," in *Annals of Telecommunications*, vol. 63, no. 5, pp. 253-269, 2008

[8] R L Cruz and AV Santhanam, "Optimal routing, link scheduling and power control in multi-hop wireless networks," in *Proceeding of the IEEE International Conference on Computer Communications*, pp. 702–711, 2003

[9] A Behzad, I Rubin, "Optimum integrated link scheduling and power control for multihop wireless network," in *IEEE Transactions on Vehicular Technology*, vol. 56, no. 1, pp. 194-205, 2007

[10] A Behzad, I Rubin, J Hsu, "On the performance of the randomized power control algorithms for random multiple access in wireless networks," in *Proceedings of the IEEE Wireless Communications and Networking Conference*, pp. 707-711, 2005

[11] W Liang, "Approximate minimum-energy multicasting in wireless ad hoc networks," in *IEEE Transactions on Mobile Computing*, vol. 5, no. 4, pp. 377-387, 2006

[12] J Wieselthier, G Nguyen, A Ephremides, "On the construction of energy-efficient broadcast and multicast trees in wireless networks," in *Proceeding of the IEEE International Conference on Computer Communications*, pp. 585–594, 2000

[13] A Behzad, I Rubin, "High transmission power increases the capacity of ad hoc wireless networks," in *IEEE Transactions on Wireless Communications*, vol. 5, no.1 pp. 156–165, 2006

[14] TS Rappaport, *Wireless Communications: Principles and Practice*, 2nd Ed. (Englewood Cliffs, NJ: Prentice-Hall, 2002)

[15] B Noble, J Daniel, Appied Linear Algebra, 3rd Ed. (Englewood Cliff, NJ: Prentice-Hall, 1988)

[16] N Bambos, SC Chen, GJ Pottie, "Radio Link Admission Algorithms for Wireless Networks with Power Cotnrol and Active Link Quality Protoction," in *Proceeding of the IEEE International Conference on Computer Communications*, pp. 97-104, 1995

[17] M Pursley, H Russell, and J Wysocarski, "Energy-Efficient Transmission and Routing Protocols for Wireless Multiple-hop Networks and Spread-Spectrum Radios," in *IEEE/AFCEA EUROCOMM 2000, Information Systems for Enhanced Public Safety and Security*, pp. 1-5, 2000

[18] M Halldorsson and J Radhakrishnan, “Greed is Good: Approximating Independent Sets in Sparse and Bounded-Degree Graphs,” *Algorithmica*, vol. 18, no.1, pp. 145-163, 1997

[19] TH Lee, JC Lin, and YT Su, “Downlink power control algorithms for cellular radio systems, IEEE Transactions on Vehicular Technology,” vol. 44, no.1, pp. 89-94, 1995

[20] 3GPP TS 36.300 V9.1.0, “Technical Specification Group Radio Access Network; Evolved Universal Terrestrial Radio Access Network (E-UTRAN); Stage 2,” Rel. 9, 2009

[21] VS Abhayawardhana, IJ Wassell, D Crosby, MP Sellars, MG Brown, “Comparison of empirical propagation path loss models for fixed wireless access systems,” in *Proceedings of the IEEE Vehecular Technology Conference*, pp. 73-77, 2005

[22] A Alexiou, C Bouras, V. Kokkinos, G. Tsichritzis, “Spectral efficiency performance of MBSFN-based LTE networks,” in *Proceedings of the IEEE International Conference on Wireless and Mobile Computing, Networking and Communications*, pp. 361-367, 2010

4 Dynamic Unicast Scheduling Algorithm for Failovers and Heterogeneous Loading in Cellular Wireless Networks

Cell outage management is a functionality that aims to automatically detect and mitigate outages that occur in cellular networks due to unexpected failures, and is an integral part of the Self-Organizing Network [1]-[3] concept for LTE systems [4],[5]. It is essential that the system has the capability to compensate for possible outage-induced coverage reductions and performance degradations during network failure events, such as the failure of base stations.

Various unicast services with failover considerations have been previously studied. In [6]-[8], the authors adjust the pilot power, antenna tilt and azimuth to mitigate outage-induced performance degradations. The study in [9] automatically reconfigures the neighboring base stations of the failed cell by adjusting their transmit power levels for outage compensation. However, these papers neither consider changing the scheduling patterns used by base stations, nor transmission rate adaptations, when compensating for loading asymmetries induced by cells with distinct loading rates or by observing such differences induced by base station nodal failures.

For unicast services without failover considerations, [16], [17] use scheduling algorithms by carrier assignment (bandwidth allocation) with BS cooperation considerations but without adaptive rate and power. [18]–[20] propose scheduling algorithms with BS cooperation and power adaptations without adaptive rate, where [18] operates static 3-coloring and 4-coloring frequency reuse scheme and [20] considers frequency reuse-1 and reuse-3 scheme. [21] utilizes scheduling algorithms with BS cooperation, adaptive power and bandwidth allocation in static reuse-1, static reuse-3 and static and dynamic of mixed frequency reuse-1 and reuse3 scheme but without adaptive rate. [22] considers some important issues (e.g., the ACK/NACK error rate and

the effect of control signaling resources limitation) in unicast service but without scheduling considerations.

We aim to develop scheduling algorithms derived through coordination among base station (BS) nodes, incorporating into the operation cross-layer code rate adaptations that are achieved by the dynamic selection of the proper modulation/coding schemes (MCS). Mobile stations are randomly distributed in the region covered by the cellular wireless BS nodes. These BS nodes aim to transmit the messages that they received from a backbone network to the corresponding destination mobiles along prescribed downlink channels. We assume that through the use of an established feedback control channel, each mobile keeps its associated BS node aware of its location and measures relevant signal-to-interference-and-noise ratio (SINR) related to its BS node. We aim to calculate the maximum achievable levels of throughput rate (identified as the throughput capacity) of the system, when considering a region covered by BS nodes, assuming that base stations assure mobiles with a measure of fairness. To assure fair service, we require a BS node to assure mobiles in each sector with its fair level of service (so that when all sectors are busy, each receives an equal measure of capacity). We also assure the transmission of downlink messages by a BS to mobiles located within a cell sector to proceed in a manner that does support mobile preference based on mobile locations within the sector.

We present scheduling algorithms that allocate time slots, over a prescribed frequency band to be employed, to base stations for the downlink transmission of their messages. When the system is symmetrically loaded, or when it is highly loaded such that all BS nodes are kept fully engaged, we employ a sector oriented time-reuse *static* scheduling protocol under which all BS nodes are scheduled to transmit their messages to mobiles in cell sector i during time slot i. In turn, when the system is asymmetrically loaded, such that in each neighborhood there may be a

cell (or several such BS nodes) that is heavily loaded while the rest are lightly-loaded, the use of the static scheduling algorithm is much improved by the use of a dynamic scheduling algorithm. We introduce two such mechanisms that readily adapt to asymmetries in system loading conditions. One of these mechanisms, identified as the *adaptive* scheduling scheme, is quite complex and is thus used to provide for a calculation of an upper bound on the throughput capacity rate achieved through the use of a lower complexity algorithm. The latter, identified as the *dynamic* scheduling algorithm, is based on the following concept. A heavily loaded BS node is permitted to execute downlink message transmissions to mobiles that are located in sector i, by not only using its *native* allocated time slot i, but also making use of time slot j, where $j \neq i$. The latter transmissions, which take place during a *non-native* time slot, can only be executed when they do not interfere with downlink transmissions of other BS nodes that would take place during their allocated native time periods.

In addition to the introduction of this scheduling scheme, we also carry out performance analyses and evaluations, proving that the dynamic mechanisms lead to significant enhancement of the system throughput capacity. Furthermore, we show this dynamic algorithm to also exhibit efficient behavior under the failure of a base station node. In this case, neighboring BS nodes adapt their scheduling operations (and selected code rates) to provide coverage to mobiles that are located in the area of the failed cell.

The system model is presented in Section 4.1. In Section 4.2, we present our adaptive and dynamic scheduling algorithms, and assess the complexity of the algorithms in Section 4.3. We then perform analyses of these schemes, considering pre-failure and post-failure operations, under different asymmetric traffic loading levels in Section 4.4. In Section 4.5, we evaluate the performance behavior of the system under different scheduling schemes by simulation. We

demonstrate the distinct performance enhancement attained under the use of the dynamic scheduling protocol.

4.1 System Model

We consider cellular wireless networks whereby base stations are interconnected through a backbone network, and each cell is managed by a macro base station, such as LTE networks. Neighboring base stations are time slot synchronized, sharing their downlink channels on a coordinated spatial-TDMA basis. To simplify the presentation of our analytical model, we assume the time slot duration to be equal to the transmission time of a prescribed load of messages under the lowest acceptable SINR level and the corresponding data rate level (under a prescribed bit error rate value). Regional neighboring base stations interact with each other for the purpose of coordinating this TDMA schedule (note that similar analyses and protocols apply when combined time/frequency allocations are utilized and coordinated).

A downlink control channel is available and employed in each cell, allowing each BS node to periodically transmit control signals to its mobiles, as well as to neighboring BS nodes, identifying their joint configuration of downlink transmission schedules. Uplink control channels are used by the mobiles to associate with their selected BS node and to update the latter about their location and SINR related metrics. In this manner, mobiles continuously monitor the quality of their reception channels, reporting to their associated BS nodes the channel quality information (CQI) status. BS nodes use this information to derive the propagation gains for their downlink channels. We assume here that such updates are executed at a sufficiently fast pace to be of relevance for the time period over which the underlying scheduling operation is performed. Note that the CQI collection mechanism is part of the LTE infrastructure, and is included in the control plane [17].

We assume that BS nodes to employ tri-sectored antennas. Each BS node is capable of adjusting its transmit power level continuously in the range [0, P_{max}]. Under a given SINR level at the intended mobile's receiver, base station select from a prescribed database of available encoded MCS implemented within the system (as defined in [21]) and the corresponding data rate for each downlink message transmission that is targeted for reception by this mobile.

To simplify our illustrations and analysis, we assume the channel propagation gain to be modeled as $G_{ij} = K/d_{ij}^{\alpha}$, where d_{ij} is the distance between the transmitting base station i and receiving mobile j, α denotes the path loss exponent, and K is a factor that accounts for absorption and penetration losses. This model and related parameters are customarily employed for the modeling, analysis and design of cellular wireless network systems, such as LTE systems (see [17] - [21]). We assume the propagation gain matrix to be fixed during the period for which the schedule is calculated. We have also studied the behavior of the system when the communications channels are subjected to slow shadow fading effects (characterized by Log-Normal distributions, as customarily assumed for many LTE systems). While such fading phenomena lead to reduced throughput rate levels, they do not vary much our conclusions about the efficiency of the dynamic scheduling scheme studied here, when compared with a corresponding static scheduling scheme; thus we do not include such phenomena.

4.2 Dynamic Scheduling Algorithms

In this section, we introduce our dynamic scheduling algorithms and failover schemes. The first algorithm to be presented is a static coloring based scheduling algorithm, whereas the other two algorithms are our dynamic scheduling algorithms. The static scheduling algorithm is used as a baseline reference in comparing the throughput capacity gains that are achieved by employing the adaptive and dynamic algorithms. The static algorithm also identifies the

throughput capacity achieved by the system when it is symmetrically loaded (across distinct cell areas) as well as when it is uniformly overloaded.

4.2.1 Static Coloring Algorithm (SCA)

We assume a TDMA oriented operation, such that under a *k*-color scheduling scheme, a time frame consists of *k* time slots. We consider a static 3-color scheduling scheme as shown in Fig. 4-1, whereby each color identifies a separate spatial cell sector, accounting for the tri-sectored antennas of the BS nodes. BS nodes transmit at their max power level. A BS node transmits messages that are directed to mobiles residing in its sector *i* during time slot *i* (corresponding to color *i*), for *i* =1,2,3. We assume that BS nodes coordinate and synchronize the coloring of their time slots, so that other BS nodes that direct their transmissions to mobile located in the same sector-directionality in time slot *i* transmit in a time simultaneous fashion such messages (i.e., a reuse-1 operation per cell sector).

BS nodes downlink transmission rates are adapted by adjusting the employed code rate of the MCS in accordance with the SINR monitored at receiving mobiles. When system loading at different cells is subjected to asymmetric patterns, we note the following. During certain time periods, a BS node may discover that its neighboring cells are lightly loaded such that its mobiles report lower signal interference levels, and thus higher SINR values. This base station will then adjust the MCS so that higher code rate are properly configured leading to higher throughput capacity rates. However, due to the static nature of the scheduling scheme, a busy BS node is not allowed to transmit messages to mobiles located in sector *i* during time slot *j* even if the latter time slot is not utilized by any interfering BS node, and therefore wasting the opportunity of enhancing its throughput capacity level. Also, under the failure of a BS node, the loading of different base stations is driven in an asymmetric manner. The BS nodes that neighbor the failed

cell are now assigned to provide coverage to mobiles that reside in that cell. Such BS nodes are now tasked with the support of higher traffic rates, leading to asymmetric traffic loading conditions. The dynamic scheduling schemes presented by us in the following sections provide for adaptive utilization of channel resources and thus attain much higher throughput capacity levels under such asymmetric traffic loading scenarios.

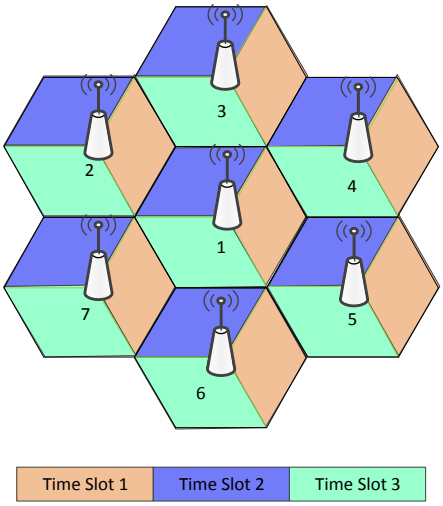

Fig. 4-1: Static 3-Color Scheduling Scheme

4.2.2 Adaptive Scheduling Algorithm (ASA)

In this section, we present an Adaptive Scheduling Algorithm (ASA). This implementation mechanisms required by this algorithm is quite complex, and our objective here is to use this algorithm to provide us with a upper bound on the throughput capacity rate that is attainable when rate adaptive operations are enacted under asymmetric BS traffic loading conditions. Consequently, we proceed in the following to describe just the key elements of the scheme, without engaging in detailed design issues.

Under this adaptive scheduling algorithm, the following process is continuously invoked. Each BS node calculates periodically (each time frame, or every batch of frames), for mobiles currently located (or estimated to be located) in each one of its cell sector, a “weight” metric that

is equal to the average time that it would take to transmit messages to these mobiles, per slot. In performing this calculation, the average rate and transmission time are computed by noting that mobiles are distributed over the sector, so that a BS node can transmit at higher rates to mobiles that are located closer to it. Note that other weight metrics can also be utilized, in expressing the overall throughput rate, averaged per slot, required per sector by the BS node to meet its current loading pattern. Each BS node then periodically advertises over the control channel its current weight metric $w(t,i)$, for time t and sector i, for each sector, within its 2-hop BS neighborhood. BS nodes compare their own and advertised weights. The BS nodes that have the highest weight metrics in their neighborhood (having at most one such per neighborhood) are declared as the current winners. They are scheduled to transmit their messages in this time slot (which is under consideration).

Based on the interference and noise levels reported by its mobiles, each winning base station calculates the current SINR level incurred at its receiving mobiles. Since each scheduled mobile is guaranteed to receive its base station's signal at a SINR level that is higher than the required SINR threshold, the difference between the latter two identifies the current power margin level associated with signal reception at each mobile. This power margin value identifies the amount of additional interfering power that a covered mobile is able to sustain, without violating its receive SINR level requirement. Each winning base station proceeds to advertise to its BS neighbors the list of such interference power margins. The announced interference power margin levels impose constraints on the transmit power level that can be employed by base stations that are to be considered in the next iteration for possibly scheduling their transmissions to take place during the same time slot.

Unscheduled base stations consequently calculate their highest feasible transmit power level, and announce to their neighbors their newly modified weight metrics. The next winning base station (if any), is subsequently selected and scheduled to transmit at this same time slot at its calculated allowable maximum transmit power level (making sure that they do not violate the announced interference signal power margins announced for mobiles that have already been scheduled to receive messages during an earlier step of this iteration process). The iteration process continues in this manner until the interference power margin levels advertised for already scheduled to receive (covered) mobiles are not sufficiently high to permit an operation that accommodates the scheduling of an additional base station in this time slot. If there are still mobiles to be covered, the algorithm continues to schedule transmissions in the subsequent time slot, using the same approach. A flow diagram that outlines the process used by ASA is shown in Fig. 4-2.

When a base station failure is detected, the algorithm will automatically attempt to adjust the transmit power and rate levels of base stations that are neighbors of the failed cell while synthesizing a new transmission schedule for all base stations, using the same approach as described above. Mobiles that are located in the failed cell area are subsequently associated with and scheduled by their new associated BS node. Since the derivation of an optimal solution to this problem is NP-hard [18], we develop a more computationally efficient heuristic algorithm for such coordinated adaptive scheduling mechanism.

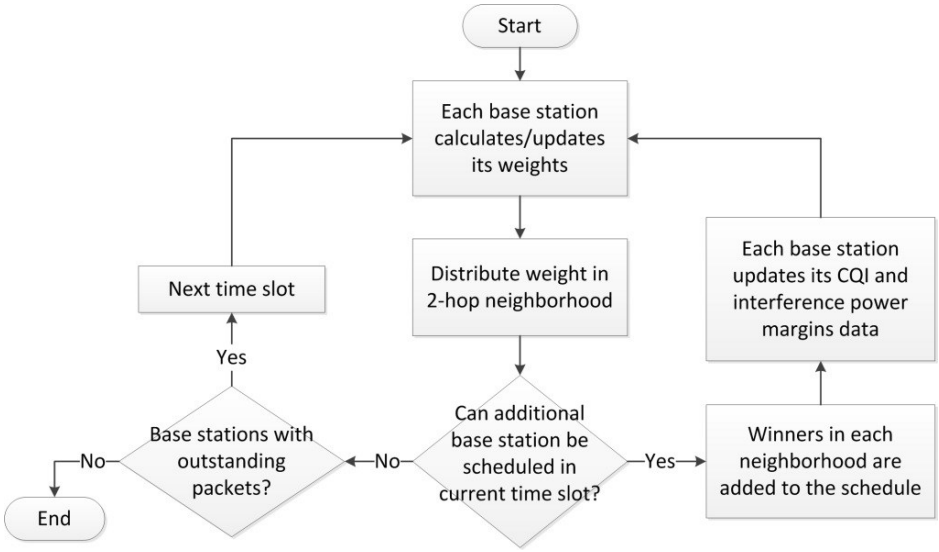

Fig. 4-2: Flow Diagram of Adaptive Scheduling Algorithm (ASA)

4.2.3 Dynamic Coloring Algorithm (DCA)

In this section, we introduce and describe a scheduling algorithm that is much simpler to implement when comparing with ASA presented in the previous section. Our aim is to use a relatively simple and easy to implement scheduling mechanism that employs a coloring based scheduling procedure, as commonly implemented by cellular wireless network systems. However, we introduce into this coloring based scheduling algorithm provisions that will allow BS nodes that experience high traffic loading levels to take advantage of communications capacity resources that become available during periods of time in which some of their neighboring BS nodes experience lighter traffic loading levels. This is encountered quite often in situations that involve heavily-loaded cells that are surrounded by cells that experience during certain periods of time much lighter traffic loading conditions. This algorithm is identified here as the Dynamic Scheduling Algorithm (DSA). To simplify the operation, this protocol excludes the use of power adaptation.

We aim to assure each cell with a guaranteed minimum service level. For this purpose, assume that under symmetric loading conditions, or when BS nodes are overloaded, the

scheduling mechanism is identical to that employed by SCA. Thus, each BS node, for the purpose of transmitting its messages across the downlink to its mobiles that are located in cell sector *i*, is given priority to using its slot *i*. These slots, as used in this manner, are identified here as the BS's native time slots. Under the scenario when al BS nodes have high loading levels, each BS node realizes in each sector a throughput level of 1/3 [Erlangs], being guaranteed to make use of the downlink in this sector for one third of the time. The average rate of transmissions, E[R] realized by the BS node in each sector, is calculated based on the distributions of the SINR levels advertised to it by its mobiles that reside in the sector. Thus, the throughput capacity rate achieved by a BS node when using its native slots is thus equal to E[R]/3 [bps/sector].

In turn, when the system is not overloaded and when cells are asymmetrically loaded, the DSA protocol allows busy BS nodes to utilize non-native time slots for the downlink transmission of their messages. However, to permit a BS node to occupy a non-native time slot, two non-interference condition (NIC) checks must be performed and return with positive results. The checks are defined as follows.

4.2.3.1 NIC Check 1: Non-interfering Conditions Met by the Activity of Neighboring Cells during Native Time Slots

A BS node that has residual messages for transmission to mobiles that reside in sector *i*, in a current frame (i.e., it has more messages to transmit than can be accommodated by transmissions carried out during its native slot) may make use of a non-native slot *j* for such transmissions if the corresponding NIC Check 1 returns a positive result. The latter requires the BS node to verify that its transmissions during non-native slot *j* would not interfere with receptions scheduled to take place in neighboring cells during slot *j*. To simplify such a check, we assume it involves verification that neighboring BS nodes that are scheduled to use their native slot *j*

during this frame, currently have no such messages to transmit. It is noted that this check can be performed periodically at designated times, based on announcements made by the neighboring BS nodes as to their loading levels in reaching mobiles in each cell sector. For example, a neighboring BS node may announce itself to have traffic loads that requires over the next N frames the use of only its native time slots, and is busy only during a specified subset of slots included in this period of N frames. In the following, we show that NIC Check 1 involves asserting the activity plans of three neighboring BS nodes.

Property 1: NIC Check 1 entails verifying that three BS nodes, whose identities are specific to the non-native time slot being considered, are inactive during the underlying time frame(s).

***Proof*:** As observed in Fig. 4-3, consider the transmission messages by BS1 to mobiles that reside in cell sector 1. Allocated native time slot TS1 will first be used for this purpose. If a backlog of messages destined to mobiles located in sector 1 is detected at BS1, the algorithm instructs BS 1 to check whether it can also transmit these messages during non-native time slots (i.e., during TS2 and TS3). Under NIC Check 1, BS1 must ensure that BS3, BS4, and BS5 do not have messages to send during their native TS2 slots:

(a) If, during the underlying frame, BS3 and BS4 have messages to transmit in their native TS2 slots, then their transmissions will interfere with the transmissions of BS1 if scheduled to occur during its non-native TS2 slots, as shown in Fig. 4-2(a). Such interference is identified by us as transmit-based interference (Tx-Interference).

(b) If BS1 were allowed to transmit messages in non-native TS2 slots, then its transmissions will interfere with transmissions conducted by BS4 and BS5 during their native TS2 slots, if any, as shown in Fig. 4-2(b). Such interference is identified by us as receive-based interference (Rx-Interference).

Thus, as long as conditions (a) and (b) are enforced, NIC Check 1 assures the desired non interference condition to be met during non-native TS2. Similarly, plans for transmissions by three neighboring BS nodes must be checked by BS1 prior to allowing its use of non-native TS3. QED

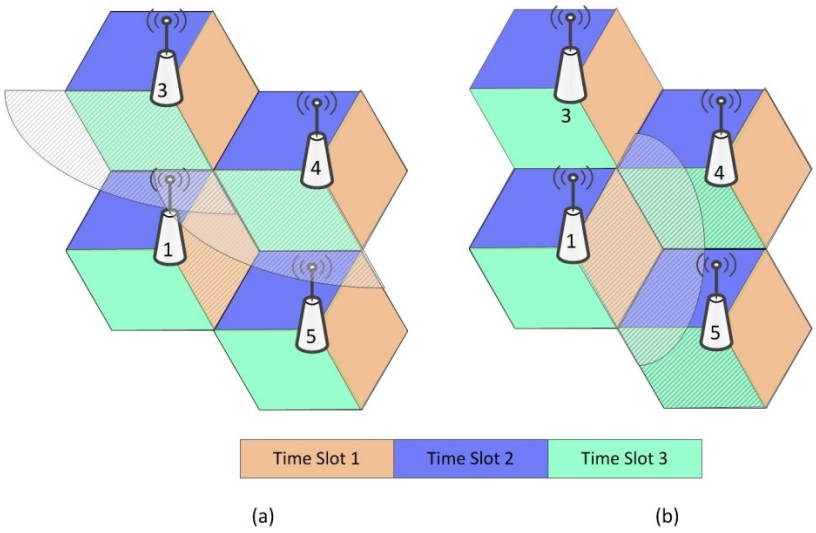

Fig. 4-3: Layouts illustrating the selection criteria used for DSA when BS1 is not able to transmit during non-native Time Slot 3

4.2.3.2 NIC Check 2: Conflict Resolution when Multiple Neighboring BS Nodes Plan to Use Conflicting Non-Native Slots

Based on the checks made in accordance with the rule specified by NIC Check 1, it is possible that multiple neighboring BS nodes may determine that they are permitted to use the same non-native time slot. If they proceed with such transmissions, this may lead to interferences at destined mobiles. In Fig. 4-4, we illustrate a scenario under which it is possible that multiple neighboring BS nodes determine that they are permitted to transmit in the same non-native time slots. From NIC Check 1, BS1 is allowed to transmit to mobiles in sector 1 during non-native TS3 slot after checking with neighbors BS4, BS5 and BS6. Alternatively, BS4 is allowed to transmit to mobiles in sector 2 during non-native TS3 after checking with

neighbors BS1, BS5 and BS8. If both BS1 and BS4 proceed with these selected non-native transmissions, their corresponding simultaneous transmissions will cause signal interference at the destined mobiles.

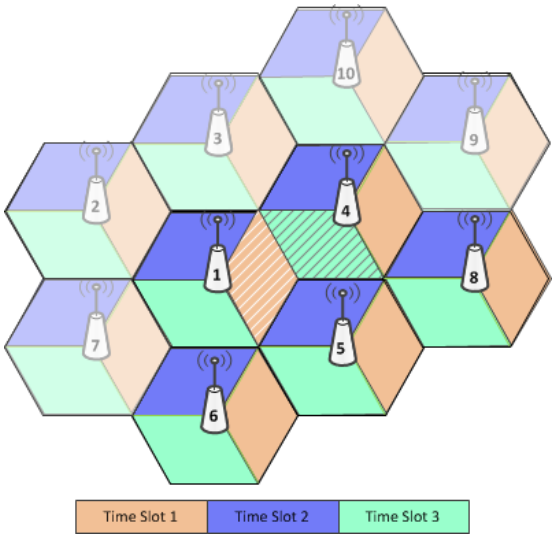

Fig. 4-4: Conflicting Non-Native Time Slot Transmissions

To resolve such conflicts, we set the following resolution procedure as NIC Check 2. We require BS nodes that are determined through the use of NIC Check 1, which can use a non-native time slot, to check whether during this time slot other BS nodes also plan to execute transmissions using their non-native time slots. If so, each BS node must make sure that the transmission in each one of the non-native time slots that it plans to use, does not lead to Tx-Interference and to Rx-Interference with any one of its neighboring BS nodes. As described above, each such check, when considering a non-native time slot, involves checking the transmission plans advertised by two sets of two neighboring BS nodes. If any such conflict arises, the stations cancel their plan to use the underlying non-native time slot. Otherwise, the BS node will proceed to use its non-native time slot, as planned. Clearly, each BS node notifies periodically each one of its neighboring BS nodes as to its plans to make use of its non-native time slots, so that NIC Check 2 can be readily carried out at each BS node.

To resolve such conflicts while assuring fair access to different BS nodes to the use of excess capacity resources, we have evaluated the performance of the system when a round-robin based resource allocation rule is employed. In this manner, BS nodes keep a running record of such conflicts with other neighboring BS nodes, so that BS nodal winners are jointly elected in a cyclic fair manner. In addition, we have also studied such systems when weighted round-robin scheme is used, under which BS nodes that serve cells with a higher number of mobiles (which leads to higher loading rates) were assigned higher weights. Note that other fairness oriented distribution rules can be applied in a similar manner. The conflict resolution described above leads to the following result.

Property 2: Under NIC Check 2, each BS node determines whether it should proceed to use specific non-native times slot, by examining the plans advertised by two sets of neighboring BS nodes (Tx- and Rx-Interference sets, each of which consists of two BS nodes). If conflicts arise, a fairness rule is applied to determine which BS node is allowed to use the corresponding non-native time slot.

Note that for illustration purposes, and to attain higher throughput rates, we assume that each base station employs three radios, allowing it to simultaneously transmit messages across multiple cell sectors during the same time slot.

4.3 Complexity Analysis of the Dynamic Scheduling Algorithms

In this section, we show that the computational complexity of our heuristic dynamic algorithm is of polynomial order. Assume there are M base stations in the network. Assume that each base station has 3 sectors, B neighboring base stations and C mobiles residing in each cell sector. Under ASA, each base station calculates its weight level with an order of $O(BC)$ calculations. Each base station then compares its weight level with the weight values announced

by other base stations, determining whether its weight level makes it a current winner. During the contention phase, each contending base station compares its weight level only with those announced by base stations that are in its 2-hop BS neighborhood (which are of the order of $B^2 < M$). The number of iterative calculations executed in each time slot is of the order of B^2. We note that the schedule (serving the given load) will be completed after a finite number of time slots (K) is assigned, noting that generally $K = O(M)$. Hence, the computational complexity of ASA is of the order of $O(MB^4) + O(MB^3C)$. The computational complexity for this scheme increases when it is determined that the selected transmission is not feasible, since the recently scheduled base station must be dropped from the schedule, and the contention phase must be re-run. At any rate, it is still of the order of the number of base stations residing in the 2-hop BS neighborhood, as used for the complexity bound noted above. However, the occurrence rate of such events is generally determined to be low, assuming that a sufficient interference margin is accounted for during the design.

Under the dynamic coloring algorithm, as long as they are busy with messages, BS nodes are allowed to schedule their transmissions in their allocated native time slots. To support its backlogged messages, a BS node determines whether it can use its non-native time slots by running NIC Checks 1 and 2. Each BS checks its traffic loading for each of its cell sector, a computation whose complexity is merely of the order of $O(C)$. Each NIC check requires a constant number of calculations, and the number of iterative calculations executed in each time slot is also constant. Hence, the computational complexity of DCA is of the order of $O(MC)$.

Property 3: The iteration process employed by the two dynamic algorithms terminates after a finite number of steps with a feasible schedule.

***Proof*:** Under ASA, for each iteration step involving scheduling transmissions in a given time slot, each residual base station node executes the computation of a weight metric. A simple resolution scheme is employed in case of ties (such as applying the BS node's ID). The election procedure then yields a single winner. It is the one that announces the highest metric level in each contending BS neighborhood. The winner is added to the schedule if it passes the feasibility test. The subsequent test period requires mobiles to measure the underlying SINR levels and report back to their base stations, affirming (or not) the feasibility of allowing other BS nodes to schedule transmissions during this time slot. It is noted that during each iteration step executed in attaining a schedule in a time slot, when the process has not been terminated, at least a single new transmission is added into the schedule involving allocations made in this neighborhood. Furthermore, the addition of new transmissions to an existing schedule in each time slot is executed only if it guarantees the continued feasibility of existing transmissions, therefore avoiding assignment cycles.

For DCA, each BS node is guaranteed allocation of its native time slots, when required. Only BS nodes that contain cell sectors that are loaded with excess traffic rates (i.e., more than 1/3 [Erlangs]) will try to make use of the non-native time slots. The use of the NIC Checks 1 and 2 assures the feasibility of carrying out non-native transmissions under DCA. These NIC checks result in a unique resolution after a finite number of steps, since each one of the finite number of BS nodes that are involved in performing the checks, executes a limited number of computations, in connection with only three distinct possible neighboring BS nodes, for evaluation of possible conflicts that may arise in the use of each one of its non-native time slots, when of interest. If it determines that such conflicts exist, a fairness rule is applied, resulting in a distributed determination of an agreed upon winner, based on a running record of usage for each one of its

neighboring BS nodes. We have assumed an area of operation that involves a finite number of base stations, so that the complete scheduling process involves a finite number of steps and time slots. QED

4.4 Performance Analysis

4.4.1 Pre-Failure Analysis

Under the cellular network layout, BS nodes are assumed to use tri-sectored antennas. We assume each BS node to be assigned a single slot per frame for its downlink transmissions, based on the use of a commonly employed 3-color based scheduling scheme. In this manner, assuming a time frame that consists of 3 time slots, time slot 1 (TS1) is used by all BS nodes in the area of operations to simultaneously transmit messages that are destined to mobiles that reside in their cells under the coverage of antenna sector 1 (such as the colored sector in Fig. 4-5). Similarly, time slots TS2 and TS3 are used by BS nodes to transmit messages to mobiles that reside in their cell sectors 2 and 3, respectively. For simplified presentation, we assume equal time slot durations.

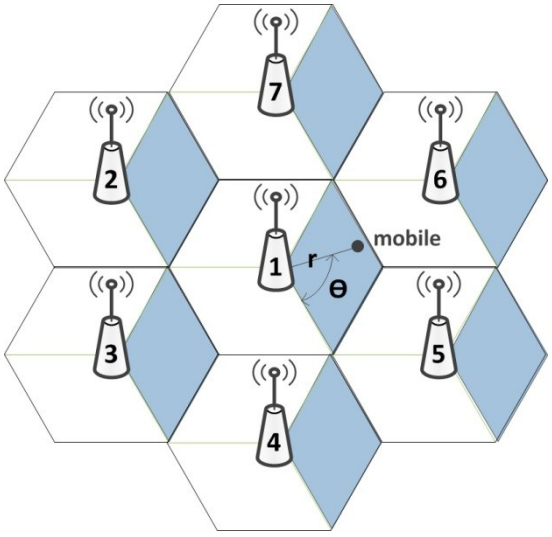

Fig. 4-5: Interferences from two neighboring cells under 3-color based scheduling

Assume message arrivals at each base station to follow the statistics of a Poisson process. The arrival rates of messages at base stations $BS_1,\ldots,BS_n$ are denoted as $\lambda_1,\ldots,\lambda_n$, respectively. We define the parameter gamma, $\gamma = \lambda_n/\lambda_1$, to denote the ratio between the highest and lowest message arrival rates; it thus measure the level of loading asymmetry in the network. We assume that a BS node adjusts the code rate (and the corresponding selected MCS) utilized for the transmission of its messages to a specific mobile in accordance with the corresponding SINR level advertised by this receiver. Assuming the use of Shannon's capacity formula for AWGN channels (noting that one can similarly set the model to apply specific code rates of the selected MCS), and assuming mobiles to be randomly and uniformly spatially distributed over the cell area (and thus following the spatial density $f(r,\Theta)$ shown below), we calculate the average rate E[R] used for message transmissions to mobiles in a cell's sector to be expressed as:

$$E[R] = \int_{\pi=0}^{\frac{2\pi}{3}} \int_{r=0}^{R} log_2\big(1 + SINR(r,\theta)\big) G(\theta) f(r,\theta) d\theta dr$$

$$= \int_{\pi=0}^{\frac{2\pi}{3}} \int_{r=0}^{R} log_2\big(1 + SINR(r,\theta)\big) G(\theta) \left(\frac{2\pi r}{\pi R^2} dr\right) \left(\frac{3}{2\pi} d\theta\right) \quad (4\text{-}1)$$

where SINR(r, Θ) is the Signal to Interference plus Noise Ratio monitored at a receiving mobiles that is located at (r, Θ). The parameters r and Θ are polar coordinates that identify the location of a destination mobile, representing the distance and angle between the transmitting BS node and the mobiles, respectively (as shown in Fig. 4-5 for a mobile in relation to its associated BS1). We set $G(\Theta)$ to denote the relative gain of the tri-sectored antenna beam used by the BS nodes when the destined receiving mobile is positioned at angle Θ. The employed channel model accounts for an absorption level K and for distance based exponential attenuation with parameter α; for simplicity in presentation, we do not include fading components. We thus calculate the SINR monitored at a mobile as:

$$SINR(r,\theta) = \frac{P/Kr^{\alpha}}{N+\sum_{i\in B}P_i/Kd_i^{\alpha}}\ ,\ \ B = \{\text{neighboring BS nodes with key interferences}\} \quad (4\text{-}2)$$

where P is the transmit power of the base station with which the mobile is associated, N is the background noise power level as detected at the receiving mobile, P_i is the transmit power of interfering BSi, and d_i is the distance between the intended receiving mobile and an interfering BSi.

When a BS node transmits messages in its native TS1 to mobiles in sector 1, each one of its destination mobiles may be subjected to signal interferences from neighboring BS nodes that use the same time slot (and allocated OFDM frequency segment) to transmit to mobiles that are located in their own sector 1 regions. The corresponding SINR level monitored at the mobile is calculated by using Eq. (4-2), and is denoted hereby as $SINR_1$. The average rate used in the transmission of messages in this native time slot is then calculated by applying $SINR_1$ into Eq. (4-1), and is denoted as $E[R_1]$. In turn, when a BS node is permitted to transmit messages in a non-native time slot, the corresponding destination mobiles are then subjected to lower interference signals, since the use of such slots requires the meeting the NIC Checks 1 and 2 (noting the reception to be therefore mostly perturbed by ambient noise, since potentially interfering neighboring base station nodes are then noted to be idle); the corresponding measured SINR levels and transmission rates are denoted as $SINR_2$ and $E[R_2]$. Similar conditions apply when considering other time slots.

We assume BSi to be loaded with messages (destined to a mobiles in a sector) of average length $E[L_i]$ [bits] (note that the model readily applies when mobiles in different sectors receive messages that assume distinct length statistics). When transmitting such messages across a native time slot, the average message transmission time is calculated to be equal to $b_{1i} = E[L_i]/E[R_1]$ [sec]. Assuming the message arrival rate at a sector j of BSi to be identified as λ_{ij} [messages/sec],

we conclude that the Erlang loading of this sector is equal to $\rho_{ij} = \lambda_{ij} * b_{1i}$ [Erlangs]. If $\rho_{ij} \leq 1/3$ [Erlangs], on the average, this BS node can support all of this sector's message traffic load by simply using its allocated native time slot. Yet, since messages arrive in a stochastic manner, even then there may be excess instantaneous traffic loading conditions that will require the use of non-native time slots, when available. To assure fairness in the utilization of bandwidth resources by bas station nodes, we incorporate the following fairness into our dynamic algorithms: during any frame, each base station node is given precedence to the use of its native time slot for the transmission of messages to users of the corresponding sector. As noted above, each BS node announces periodically to its neighboring BS nodes concerning its activity status in planning the use of such time slots.

On the other hand, when $\rho_{ij} > 1/3$ [Erlangs], BS*i* will wish to make use of non-native transmissions to support the excess traffic destined to sector *j*, if feasible. For BS*i* to be able to transmit in a non-native time slot, it is necessary and sufficient that certain three neighboring BS nodes (as specified by the NIC checks) not have any planned transmissions in their native time slots during the time frame under consideration. When overloaded, a BS node that cannot attain the use of required excess service resources through the use of sufficient time utilization of non-native slots, can implement either a blocking or delayed service policies. Under a blocking service approach, messages that cannot be accommodated by resources made available to the BS node, during its periodic interaction with other BS nodes, are blocked and considered lost. Under a delayed service, such messages are queued and served when such resources become available, if feasible. Our mathematical models provide for approximate calculation of the throughput capacity rate (expressed in units of Erlangs as well as in units of bps/Hz/cell) for each sector served by the downlink of a BS node. This throughput capacity rate is defined as the

maximum load rate that can be supported by the base station by the underlying downlink channel used to serve mobiles that reside in the sector. Using this throughput capacity rate level as an effective sector service rate of a downlink service channel in a queueing system, we can readily calculate the message blocking probability, under a pure blocking service, or the (steady state) message delay distribution under a delayed service. For the latter case, to guarantee finite average message delay levels, the system needs to be assumed to reach steady state behavior, so that the loading rate must then be lower than the calculated service rate. We thus focus on the calculation of the throughput capacity rate behavior of the downlink sector service system when the cellular neighborhood is subjected to heterogeneous traffic loading conditions.

Let the maximum Erlang traffic loading level carried by a BS when using its allocated native time slot (and thus executing transmissions at an average rate $E[R_1]$) to be denoted as f_{static}. If all BS nodes have traffic loading levels that exceed f_{static}, no BS nodes will (on the average) be able to make use of any non-native transmissions. Under our illustrative layout, we have $f_{static}=1/3$ Erlangs. Its calculation assumes the sole use of native time slots, at an average transmission rate $E[R_1]$.

To demonstrate the mathematical modeling and analysis approach used to determine the performance behavior of the system when our dynamic scheduling algorithm is employed, we assume the following traffic distribution scenario. The analysis focuses on BS1 and the neighborhood being modeled consists of the seven cell layout shown in Fig. 4-5. To accentuate the illustration of the operation of the algorithm, and of the approach used to mathematically analyze the performance effectiveness of the algorithm, we assume BS nodes to be asymmetrically loaded in the following manner. We assume that there are only two traffic loading levels, whereby each lightly-loaded BS and each heavily loaded BS has a per-sector

offered message arrival rate $\lambda_o(L)$ and $\lambda_o(H)$, respectively. We assume a common average message length E(L) is used to characterize messages arriving to each BS node for transmission in each sector (the formulas are readily extended to scenarios where different cells or sectors carry distinct message class mixtures). Then, relative to operation at rate $E(R_1)$, which is induced by a receiving SINR monitored when a native TS is employed, we define the corresponding Erlang loading rates to be calculated as: $f_o(H) = \lambda_o(H)E(L)/E(R_1)$, $f_o(L) = \lambda_o(L)E(L)/E(R_1)$. Recalling that $\gamma = \lambda_o(H)/\lambda_o(L)$, we note that $f_o(H) = \gamma f_o(L)$.

In the following, we describe the process that we use to analytically evaluate the throughput capacity rate of systems that are asymmetrically loaded in specific ways. Our approach is to load the system at lower traffic rates and calculate the throughput rate when a potential use of non-native time slots takes place. We then compare the resulting throughput rate of the system with the offered traffic rate. As the offered rate is increased, the throughput rate tends to monotonically increase until the system reaches its throughput capacity rate level. Using this approach, the performance effectiveness of the dynamic coloring algorithm (in terms of its attained throughput capacity rate), is evaluated below for several different heterogeneous traffic loading patterns.

Case 1: Single heavily loaded BS node per neighborhood

The single heavily-loaded BS node is located in the center of the 7-cell layout. Assume all cell sectors for each BS node support the same amount traffic loading level. If the sector traffic loading level of the heaviest loaded BS node, $f_o(H)$ is less than f_{static} (on the average), non-native time slots are not required to support message transmissions since the throughput rate of the system is lower than its native capacity rate and is thus equal to the offered traffic rate. Otherwise, non-native transmissions will be utilized, when possible. The sector throughput

capacity rate achieved by a heavily loaded BS node is denoted as f_c. Since a heavily loaded BS node may make use of its native and non-native time slots, the BS node will transmit its messages at an average rate E[R], noting that $E[R_1] \leq E[R] \leq E[R_2]$. Let λ_c denote the supported message rate at a heavily loaded BS node that achieves the capacity rate. Then, we have $f_c = \lambda_c$ E[L]/E[R]. We define delta(f_c) = $f_c - f_{static}$, such that delta(f_c) represents the maximum excess carried traffic load that can be supported by a heavily loaded BS node, taking advantage (when feasible) of transmissions that are executed in non-native time slots.

The iterative process used to calculate delta(f_c,n) at iteration n is initiated (at step n=1) by setting , $f_o(H,n=1) = f_{static}$. Under such a loading rate, we have $f_c(n=1) = f_{static}$; note that the throughput rate achieved by each lightly loaded BS is equal to $f_c(n)/\gamma$. The iterative performance evaluation process then proceeds (as illustrated by the flow chart in Fig. 4-6) as follows:

1. The per-sector traffic loading level of the heavily-loaded cell, at the start of the n^{th} iteration step, is increased by an increment to $f_o(H,n) = f_{static}\,(1+n\delta)$, such that the excess offered traffic load applied to the heavilly loaded cell is $n\delta * f_{static}$. The offered load rate at each lightly loaded cell is then equal to $f_o(L,n) = (f_{static} / \gamma)\,(1+n\delta)$. The following cases are observed:
    (a) When $f_o(L,n) \geq f_{static}$, the lightly loaded BS nodes fully occupy (on the average) their native time slots so that the heavily loaded BS cannot make use of any non-native time slots.
    (b) Otherwise, when $f_o(L,n) < f_{static,}$, the heavily loaded BS can make at times use of its non-native time slots. In this case, the utilization factor for a lightly-loaded cell is denoted as $\rho(L,n) = f_o(L,n) / f_{static} < 1$. It represents the fraction of time that

a lightly loaded BS does not occupy its native time slot (and is thus also representing the steady state probability that it will not use its native slot).

2. To determine whether the heavily loaded cell can transmit messages in a specific non-native time slot, it is necessary that NIC Check 1 is satisfied (NIC Check 2 does not need to be applied for this scenario.) The probability of transmitting in a non-native time slot j is calculated as: $p(j,n) = (1-\rho_{i1,j,n})\ (1-\rho_{i2,j,n})\ (1-\rho_{i3,j,n})$, whereby i1, i2, and i3 represent the three neighboring BS nodes that are involved in NIC Check 1, and n represents the traffic loading level applied when calculating ρ in the n^{th} iteration step. Since for this layout all BS neighbors are assumed to be lightly-loaded, and are characterized by the same utilization ratio ρ, the latter probability is given as $p(j,n) = (1-\rho_{m,j,n})^3$, where $m \in \{i1, i2, i3\}$. We note that the events of the three base stations involved in the calculation not interfering are statistically independent.
3. Thus, the average excess traffic load (carried load) that can be supported by non-native transmissions executed by a heavily loaded BS for each sector depends on the number of non-native time slots that can be utilized is $\text{delta}(f_c,n) = 2\ [\ p(n)\ (1-p(n)) + p(n)^2\ ]\ f_2 = 2p(n)\ f_2$, where $f_2 = f_{static}\ E[R_2]/E[R_1]$. Note that when a heavily loaded BS node transmits its messages in a non-native time slot, it can increase its transmission rate to $E[R_2] > E[R_1]$ since the targeted mobiles now experience lower interference signals levels.

We note that, considering a base station to potentially be able to make use of its two non-native time slots, and that each non-native time slot is taken to be available for use by BS1 with probability p, or a fraction p of the time, then the 2 non-native time slots are available for use by BS1 with probability $2p$.

4. If delta(f_c,n) $\geq n\delta f_{static}$, we proceed with incrementing the offered load by δ, and moving on to the next $(n+1)^{th}$ iteration. Otherwise, the throughput capacity level has been reached, attaining: $f_c = f_{static}$ + delta(f_c, n-1).

Case 2: Two heavily loaded BS nodes per neighborhood

One heavily-loaded BS node is located at the center of the 7-cell network, and the other is positioned as one of the BS neighbors. The average excess traffic load that can be supported by non-native transmissions at the centrally-located cell is delta(f_c, n) = (1/3) $2p(n)\, f_2$ + (1/3) $p(n)\, f_2$ = $p(n)\, f_2$, whereby the outcome based on NIC Check 1 ensures that one third of the time the heavily-loaded BS nodes cannot make use of any non-native time slots, one third of the time it can make use of 1 non-native time slots with probability p, and one third of the time it can make use of 2 non-native time slots with probability $2p$. Assuming that all cell sectors are equally loaded, there will be (on the average) no collisions between non-native transmissions scheduled by the two heavily-loaded BS nodes.

Case 3: Three heavily loaded BS nodes per neighborhood

One heavily-loaded BS node is located at the center of the 7-cell network, whereas the other two heavily loaded BS nodes manage two neighboring cells. The average excess traffic load that can be supported by non-native transmissions at the centrally-located cell is delta(f_c,n) = (6/15) $p(n)\, f_2$, whereby two thirds of the time the heavily-loaded BS cannot make use of any non-native TS, 4/15 of the time it can make use of 1 non-native TS with probability p, and 1/15 of the time it can make use of 2 non-native time slots with probability $2p$.

Case 4: Four heavily loaded BS nodes per neighborhood

One heavily-loaded BS node is located at the center of the 7-cell network, and others are situated in the neighboring cells. In this case, the average excess traffic load that can be supported by non-native transmissions at the centrally-located cell reduces to almost zero.

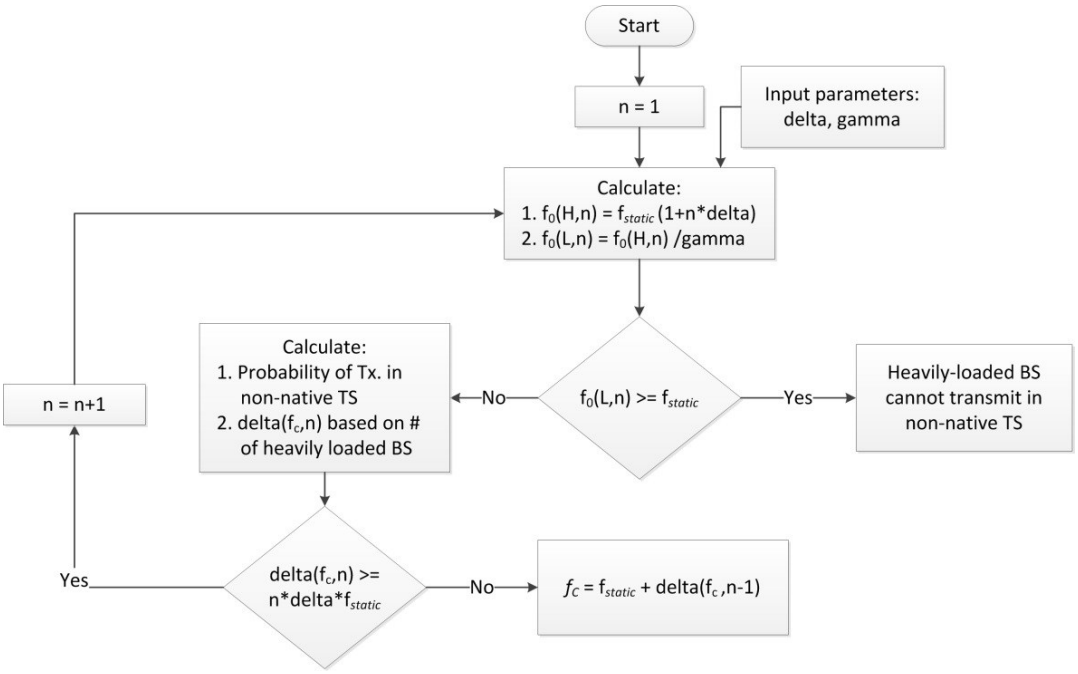

Fig. 4-6: Flow diagram for calculating the downlink throughput capacity rate attained by a heavily loaded base station

Fig. 4-7 shows the analytical and simulation performance behavior of the system, representing the attained throughput capacity rate per sector of a heavily loaded BS node vs. the number of such BS nodes, under different offered traffic loading ratio (γ) levels. We observe that the results obtained by using the analytical approximation technique are highly precise. The discrepancy between the results exhibited by the simulation and analytical calculations are attributed to the impact of interference signals received from BS nodes that are located at the second and third tiers from the receiving mobiles.

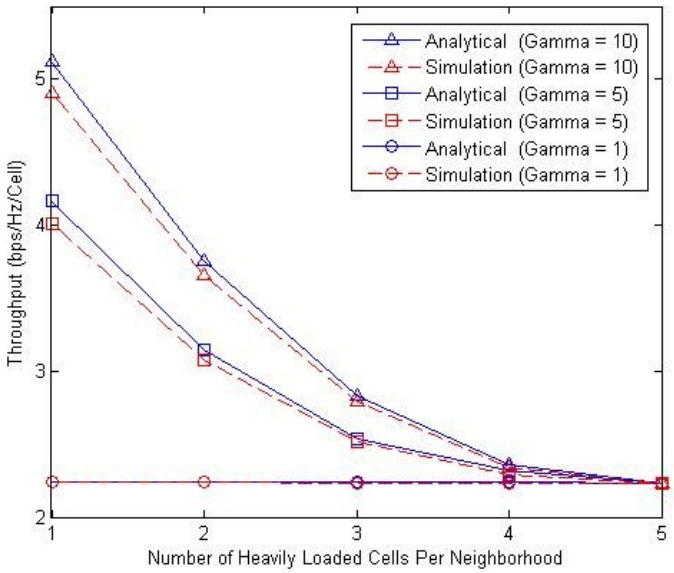

Fig. 4-7: Throughput capacity (per sector) achieved by centrally-located BS node when utilizing non-native time slots (under pre-failure scenario)

4.4.2 Post-Failure Analysis

When a BS node fails, mobiles previously supported by this failed cell will re-associate themselves to the nearest BS node, which is one of the direct neighbors of the failed cell. This scheme under which failover is handled by obtaining assistance from neighboring BSs is illustrated in Fig. 4-8. The corresponding average achievable code rate [as measured in units of bps/Hz averaged over each sector] for a given sector in a cell is calculated by using Eqs. (1)-(2). We note that our approach here is to assure downlink transmissions to each mobile, whether located in a failed cell region or not, to occur at a fair throughput rate, whereby the fairness guarantees in a post-failure system are the same as those imposed in a corresponding asymmetrically loaded system in the pre-failure scenario. In other words, in the post failure system, each BS node is guaranteed to make use of its native time slots as needed. In addition, the BS nodes that are now tasked with the support of excess mobiles that are located in the failed cell tend to require the support of higher message rate levels. In order to illustrate the

effectiveness of our dynamic algorithms under the post-failure scenario, the 7-cell network layout shown in Fig. 4-9 is examined, and we establish the throughput capacity rates per sector that are achievable in such a system.

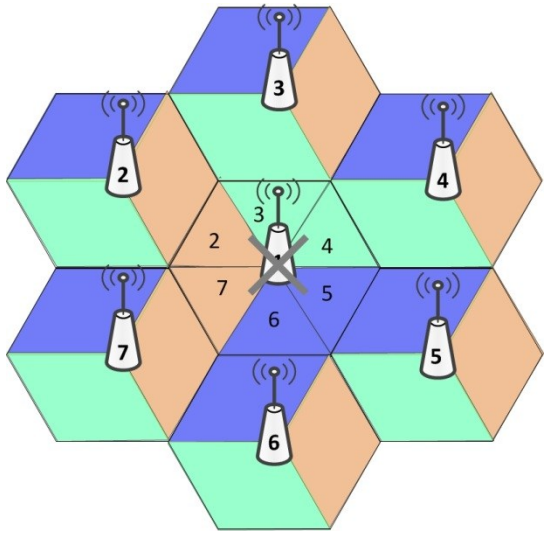

Fig. 4-8: Failover Scenario under the failure of BS1

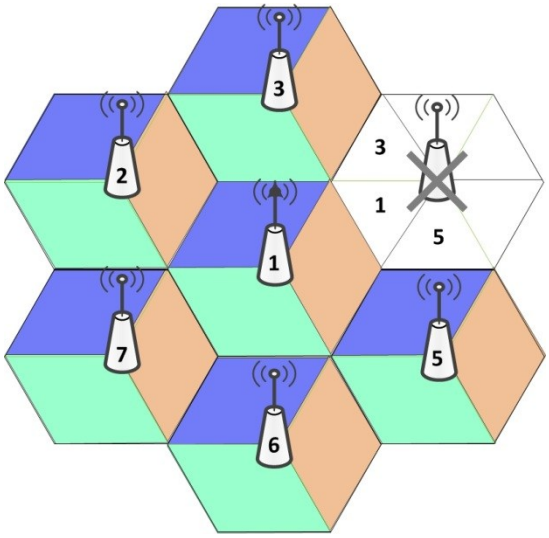

Fig. 4-9: 7-cell layout for measuring analytical throughput capacity post-failure

We assume a pre-failure scenario under which BS1 and BS4 are heavily loaded. We assume BS4 to fail. Neighboring BS1, BS3 and BS5, must now support transmission to mobiles located in the cell that was previously managed by BS4. Using our dynamic scheduling algorithms, the throughput capacity rate achieved by the centrally-located BS node utilizing non-native time

slots is calculated by using the analytical iterative procedure presented in Section 4.1.1, as well as by using simulation evaluations. The results are shown in Fig. 4-10. We compare the results with those attained for the pre-failure system, as presented in Fig. 4-7. We note that though the centrally-located BS experiences now one less interfering 1-hop BS neighbor, it is able to utilize its non-native time slots at a lower rate due to the heavier loading rates incurred at neighboring BS nodes (e.g. BS3 and BS5), which the latter must also support mobiles residing in the failed cell area. The results in Fig. 4-10 also demonstrate the capability of the dynamic scheduling algorithm to adapt to variations in traffic loads that are caused by nodal failures.

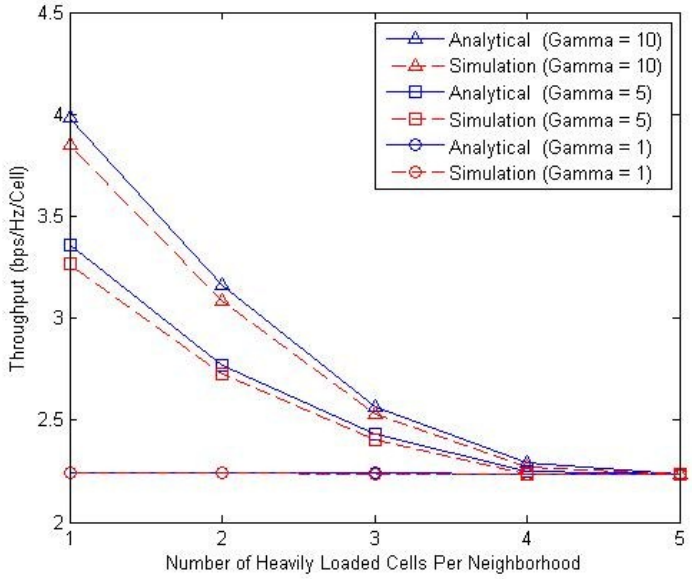

Fig. 4-10: Throughput capacity (per sector)achieved by centrally-located BS when utilizing non-native time slots (under post-failure scenario)

4.5 Performance Evaluations

To study the performance behavior of our algorithms as a function of other system parameters, we have carried out additional simulation and analysis based evaluations. We have considered a cellular wireless system with 35 tri-sector base station cells. The prescribed bandwidth is 5 MHz. Base stations are capable of adjusting their MCS (modulation/coding sets)

according to a list of such schemes as provided by an LTE specification [21]; they can adjust their power levels continuously in the range 0 to 20W (as applied by us when evaluating the performance attained by the adaptive scheduling scheme). The noise power density level is set to be -174 dBm/Hz. We have assumed in our simulations that α = 3.68 and set 10*log(K) to be −40 dB, which corresponds to a version of the urban Cost-Hata model used in LTE network studies [19]. The radius of each cell is denoted as $R = ISD/\sqrt{3}$, whereby ISD is the inter-site distance, representing the distance between two neighboring base stations. We have selected an area of geographical coverage for which ISD is set to be 500m, and the number of mobiles that are uniformly distributed over this area is assumed to be equal to 3500.

Under the pre-failure scenario, we compare the throughput of a cell as a function of γ, as shown in Fig. 4-11. We compare the performance behavior of the system, by measuring the throughput capacity rate per cell. We consider three different loading scenarios. Under Scenario 1, the centrally located cell is heavily loaded and the other cells are lightly loaded. Under Scenarios 2 and 3, we set the neighborhood to contain two and three heavily loaded cells, respectively.

When γ = 1 (uniform traffic loading across all the cells), we observe that our adaptive scheduling algorithm (ASA) achieves a slightly lower throughput performance than that attained under the static and dynamic coloring algorithms. This is because the coloring based algorithms produce more effective schedules that achieve better utilization or region-wide resources, under symmetrically loaded scenarios. Our dynamic algorithms (ASA and DCA) yield much enhanced throughput capacity rate performance behavior as the system becomes more and more asymmetrically loaded (and the γ values increase), while the static scheduling scheme is not able to efficiently adapt to such variations. The dynamic algorithms efficiently adapt their schedules

to the variations observed in the heterogeneous traffic loading layouts by allowing, when feasible, BS nodes to make use of available non native time slots for the purpose of covering mobiles in heavily used sector. The static scheme does not dynamically adapt its structure so that resources that are not utilized by their BS nodes go unused. We also observe that the performance efficiency of the DCA scheme is slightly lower than that achieved by the ASA protocol; yet, the former involves a much higher algorithmic complexity.

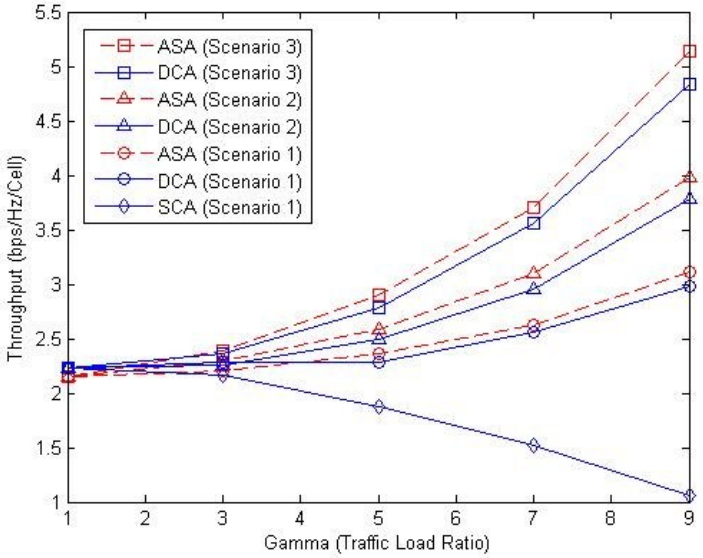

Fig. 4-11. Pre-failure Throughput Capacity Rate vs. Gamma

Following the approach described above in performing our iterative performance analysis evaluation, we proceed next to perform our simulation based evaluations. We derived the throughput capacity rates that are achievable under different traffic loading levels, by the use of our scheduling algorithms, under a given set of traffic loading levels, $\{k\lambda_1,\ldots,k\lambda_n\}$, by iteratively raising the value of k in small steps until all the BS nodes become saturated. We assume here a pure blocking service policy to be used, so that messages that arrive at a BS node when the latter does not have resources to support them are blocked and lost. The results obtained by incrementally increasing the traffic load rate at the various BS nodes, in the above described

manner (by increasing the *k* factor) are shown in Fig. 4-12. We observe that, under heterogeneous traffic loading conditions, the dynamic coloring algorithm attains much higher throughput rate levels, and throughput capacity rate values, when compared with those achieved by the static coloring algorithm.

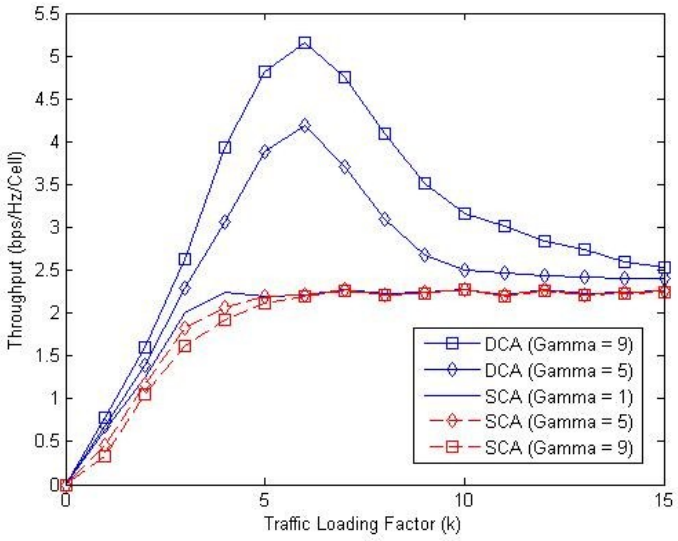

Fig. 4-12. Achievable Throughput rate (per sector) under different loading rate levels

We illustrate the system's behavior under BS failure by considering the following scenario. We assume the centrally located BS node to be the heavily loaded one, and we also assume it to fail. Following failure, neighboring BS nodes must communicate messages to mobiles located in the failed sectors. In Fig. 4-13, we compare the resulting post-failure behavior of the throughput capacity rate attained by BS nodes that support mobiles that are located in cells that are *h* BS hops away from the failed BS node. Thus, the values shown for *h*=0, represent the throughput rates attained in the support of mobiles located in the failed cell area. For a loading asymmetry ratio of $\gamma = 5$, under the failure of the central BS node, we observe that the adaptive/dynamic algorithms achieve a throughput capacity rate at the failed cell area that is 14%-25% higher than that attained by the static coloring algorithm. When $\gamma = 9$, the throughput performance of our

adaptive/dynamic algorithms at the failed cell is even further enhanced, achieving values that are 72%-116% higher than those attained by the static coloring based scheduling algorithm. In comparison, when the traffic loading is symmetrically distributed across the areas cells ($\gamma = 1$), the corresponding throughput gain attained by the use of the dynamic algorithms is noted to be equal to only about 6%-13%.

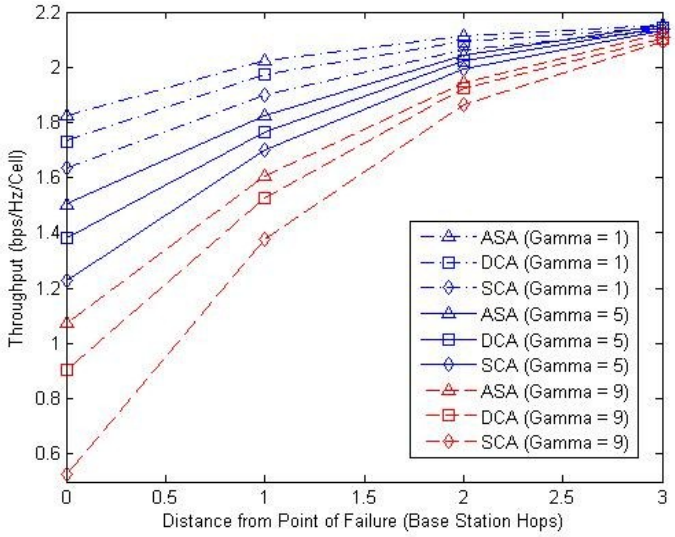

Fig. 4-13. Post-failure throughput vs. distance from point of failure

4.6 References

[1] *Evolved Universal Terrestrial Radio Access Network (E-UTRAN); Self-Configuring and Self-Optimizing Network Use Cases and Solutions*, 3GPP TS 36.902 v.1.0.1, 2008.

[2] H. Hu, J. Zhang, X. Zheng, Y. Yang, and P. Wu, "Self-configuration and self-optimization for lte networks," *IEEE Communications Magazine*, vol. 48, no. 2, pp. 94–100, Feb. 2010.

[3] J. van den Berg and et al., "Self-organization in future mobile communication networks," in *Proc. ICT Mobile Summit 08*, June 2008.

[4] *Technical Specification Group Radio Access Network; Evolved Universal Terrestrial Radio Access (E-UTRA)*, 3GPP TS 36.300 v9.1.0, 2009.

[5] *Technical Specification, Universal Mobile Telecommunications System; Introduction of the Multimedia Broadcast/Multicast Service in the Radio Access Network*, 3GPP TS 25.346 v.10.0.0, 2011.

[6] M. Amirijoo and et al., “Cell outage management in LTE networks,” in *Proc. 6th International Symposium on Wireless Communication Systems*, Sept. 2009.

[7] R. L. M. Amirijoo, L. Jorguseski and R. Nascimento, “Effectiveness of cell outage compensation in LTE networks,” in *Proc. IEEE Consumer Communications and Networking Conference (CCNC)*, Jan. 2011.

[8] M. Amirijoo, L. Jorguseski, R. Litjens, and L. Schmelz, “Cell outage compensation in LTE networks: algorithms and performance assessment,” in *IEEE Vehicular Technology Conference (VTC Spring) ’11*, May 2011.

[9] *Simulation based recommendations for DSA and selfmanagement,*, FP7 E3 project ICT-2007-216248, 2009.

[10] S.-E. Elayoubi, O. Ben Haddada, and B. Fourestie, “Performance evaluation of frequency planning schemes in OFDMA-based networks,” *IEEE Transactions on Wireless Communications*, vol. 7, no. 5, pp. 1623–1633, May 2008.

[11] *Technical Specification, Universal Mobile Telecommunications System, Physical Layer Procedures*, 3GPP TS 25.214 v.10.5.0, 2012.

[12] K. Hedayati, I. Rubin, and A. Behzad, “Integrated power controlled rate adaptation and medium access control in wireless mesh networks,” *IEEE Transactions on Wireless Communications*, vol. 9, no. 7, pp. 2362–2370, July 2010.

[13] V. Abhayawardhana, I. Wassell, D. Crosby, M. Sellars, and M. Brown, “Comparison of empirical propagation path loss models for fixed wireless access systems,” in *Proc. Vehicular Technology Conference ’05*, May 2005.

[14] L. Wang, K. Chawla, L. Greenstein, “Performance studies of narrow-beam tri-sector cellular systems,” *International Journal of Wireless Information Networks*, Vol. 5, No. 2, 1998.

[15] *LTE Physical Layer Procedures; Evolved Universal Terrestrial Radio Access (E-UTRA)*, 3GPP TS 36..213 v9.1.0 (Table 7.2.3-1), 2010.

[16] L. Chen, L. Cao, X. Zhang, and D. Yang, “A coordinated scheduling strategy in multi-cell OFDM systems”, *in Proc. of IEEE GLOBECOM Workshops*, pp. 1197–1201, 2010.

[17] H.-B. Chang and K.-C. Chen, “Cooperative spectrum sharing economy for heterogeneous wireless network”, in Proc. of IEEE GLOBECOM Workshops, 2011.

[18] G. Liu, J. Zhang, D. Jiang, L. Lei, Q. Wang, and F. Qin, “Downlink interference coordination and mitigation for future LTE-advanced system”, in Proc. of Asia-Pacific Conference on Communications, pp. 225–229, 2009.

[19] M. Pischella and J.-C. Belfiore, “Distributed weighted sum throughput maximization in multi-cell wireless networks”, in Proc. of IEEE Personal, Indoor and Mobile Radio Communications, 2008.

[20] A. Simonsson, “Frequency reuse and intercell interference co-ordination in E-UTRA”, in Proc. of IEEE in Vehicular Technology Conference, pp. 3091–3095, 2007.

[21] D. Villa, C. Castellanos, I. Kovacs, F. Frederiksen, and K. Pedersen, “Performance of downlink UTRAN LTE under control channel constraints”, in Proc. of IEEE Vehicular Technology Conference, pp. 2512–2516, 2008.

5 Conclusions

In chapter 3, we have proposed a hybrid multicast protocol that employs a mobile backbone network to achieve efficient message distribution among members of multicast groups. We combine the following three dimensions into our protocol design: *scalability*, *adaptability* and *energy conservation*. The hybrid protocol is making use of the construction of a Mobile Backbone Network (MBN) that serves to connect network nodes. Nodes that are dynamically elected to serve as backbone nodes (BNs) interact to construct a backbone network (Bnet). Under our backbone based protocols, all BNs are kept continuously awake. Other nodes are awaken only if they are part of an active session. Under the backbone flooding (BFMA) protocol, each active source floods its packets across the Bnet to all other BNs. Under the Extended Shortest Path Multicast Tree protocol (E-SPMT), an extended tree topological layout is constructed across the Bnet. We introduce an excess of BNs into the shortest path multicasting tree to attain a more robust multicasting structure. Under the hybrid protocol, a number of operational system parameters (including such that relate to the location scope of session receivers and to nodal mobility level) are measured and compared with corresponding threshold levels. Based on such comparisons, the algorithm adapts its structure to correspond to a BFMA or E-SPMT based operation. We have shown that the use of such a hybrid hierarchically structured protocol yields a much more scalable and enhanced performance behavior when compared with the performance exhibited by the commonly used flat-topology based protocol like ODMRP-PS. Through a series of simulation based evaluations, coupled with verifications based on analytical expressions of key performance metrics, we show that the MBN based hybrid multicast protocol achieves better multicast throughput rates as well as higher energy aware bit-per-joule efficiency. We have also shown our multicast protocols to achieve excellent

packet delivery ratios while producing relatively low data forwarding control overhead. Thus, the dynamic construction of a compact multicast forwarding core backbone structure is effectively utilized so that high throughput rate per consumed unit of power is achieved.

In chapter 4, we have developed efficient adaptive-power multicast scheduling algorithms for wireless cellular networks, under which base stations with multicast clients share their downlink channels, over an allocated frequency band on a spatial-TDMA basis. We model the scheduling problem as a mixed integer linear program, which is NP-hard. Consequently, we present three heuristic algorithms of polynomial complexity for solving the problem in a practical manner. The algorithms make use of the coordinated operations among time-slot synchronized area base stations which jointly interact (through the use of a central controller, or in a distributed fashion) to determine their transmission schedules and transmit power levels. Similarly, our adaptive-power scheduling algorithms lead to enhanced performance for mesh WiFi networks that use such coordination among the system access points, or mobile backbone based ad hoc wireless networks for which the elected backbone nodes employ such coordinated scheduling schemes. We show that further enhancement in throughput rate performance is achieved by using an *m-linking* operation under which, when feasible, a client may be directed to receive multicast packets transmitted by a base station which is not the same one that it is associated with. For smaller systems, our simulation results demonstrate the performance of the system, when scheduling is performed by using our first centralized heuristic algorithm, to be in the 75 percentile of that exhibited by the optimal scheme. When considering larger network layouts, we show our heuristic adaptive-power scheduling algorithms to yield a per user throughput rate that is higher than that attained by a fixed transmit power scheduling algorithm. Furthermore, our algorithms are shown to be more energy efficient than the corresponding fixed power schemes,

on a throughput per unit consumed power basis. We also show that further enhancement in the throughput rate and throughput per unit power level is attained by using our adaptive-power scheduling algorithms in conjunction with a heterogeneous network layout. In assessing the corresponding performance behavior exhibited by the illustrative LTE MBSFN multicast systems, we note our schemes to yield enhanced spectral efficiency levels when high user coverage is required, while involving much less restrictive synchronization mechanisms.

In chapter 5, we have studied the unicast message scheduling operation for failovers under heterogeneous traffic loading conditions in wireless cellular networks. We introduce a dynamic color scheduling algorithm that allows, when feasible, heavily loaded base station nodes to make use of non-native time slot allocations that are not utilized by their lightly loaded neighboring base station nodes. In comparison with a corresponding static coloring based scheduling mechanism, we show that this dynamic algorithm is able to yield a much enhanced throughout capacity behavior, when the system is subjected to heterogeneous traffic loading levels. The dynamic coloring algorithm developed and studied here is shown to be implementable in a distributed fashion through interactions by base station nodes with their 1-hop base station neighborhood. We show the protocol to impose low computational complexity requirements while achieving performance behavior that is very close to that attained by a much more complex adaptive scheduling algorithm. The presented dynamic scheduling algorithm is shown to well adapt to variations in traffic loading conditions induced by the failure of a base station node. It is thus capable of effectively mitigating outages caused by failover scenarios.